Ore Geology Reviews 124 (2020) 103639

Contents lists available at ScienceDirect

Ore Geology Reviews

journal homepage: www.elsevier.com/locate/oregeorev

Assessing the role of bitumen in the formation of stratabound Cu-(Ag) deposits: Insights from the Lorena deposit, Las Luces district, northern Chile

Andrea Herazo[a,b,*], Martin Reich[a,b], Fernando Barra[a,b], Diego Morata[a,b], Irene del Real[a,b], Anais Pagès[c]

[a] Department of Geology and Andean Geothermal Center of Excellence (CEGA), FCFM, Universidad de Chile, Plaza Ercilla 803, Santiago, Chile
[b] Millennium Nucleus for Metal Tracing Along Subduction, FCFM, Universidad de Chile, Santiago, Chile
[c] Department of Water and Environmental Regulation, Joondalup, Western Australia, Australia

ARTICLE INFO

Keywords:
Stratabound Cu-(Ag) deposits
Manto-type
Pyrobitumen
Hydrocarbons
Cu sulfides
Lorena deposit
Chile

ABSTRACT

Stratabound Cu-(Ag) deposits located in north-central Chile have been grouped into two NS parallel belts according to the age of their volcanic and volcanoclastic host rocks. Deposits from the Cretaceous belt are characterized by an unusual assemblage of Cu sulfides with migrated hydrocarbons, whereas the presence of organic matter has not yet been recognized in deposits from the Jurassic belt. Here we report the first evidence of pyrobitumen in a Jurassic stratabound Cu-(Ag) deposit and evaluate its role in ore formation. We present a micro-analytical study of pyrobitumen associated with Cu-(Fe) sulfides in the Lorena deposit, located in northern Chile. Our approach involved a combination of surface and drill core sample characterization, (FE)-SEM observations, EMPA and μ-XRF mapping of pyrobitumen. In addition, we determined the speciation of sulfur in pyrobitumen by using synchrotron μ-XANES. Two main events of hypogene mineralization were identified at Lorena deposit, i.e., a pre-ore and a main Cu ore stage. The pre-ore stage is characterized by globularly-shaped pyrobitumen and minor pyrite, and a widespread albite alteration of the andesite host rock. Pre-ore pyrite was replaced by chalcopyrite, bornite and chalcocite, providing evidence for a late Cu inception. In the main Cu ore stage, chalcocite is often associated with sharp-edged, angular pyrobitumen, most likely indicating remobilization or a later pulse of hydrocarbons. EMPA data show that pyrobitumen at Lorena is enriched in Fe (0.02–1.74 wt%), Cu (0.02–0.87 wt%), S (0.01–0.43 wt%) and Cl (0.01–0.4 wt%). Other elements detected include V, Co, Ni, Cr, Sb, As, Ag and Au. Both Ag and Au were only detected in a few spots, with Au reaching up to 600 ppm. Desktop and synchrotron μ -XRF mapping shows that S is homogeneously distributed within pyrobitumen, with lower S concentrations observed at grain rims. On the other hand, EMPA-WDS X-ray maps show that Cu precipitated on pyrobitumen grain surfaces, filling fractures and forming veinlets. In addition, textures showing the presence of micro- to nano-sized pyrobitumen inclusions within both pre-ore pyrite and main ore chalcocite grains point, unequivocally, to the interaction of hydrothermal fluids with hydrocarbons during the formation of this deposit. The high S concentrations measured in pyrobitumen and the presence of organosulfur compounds detected by μ -XANES can be attributed to an organic source. The pre-ore assemblage is interpreted as formed from a petroleum-aqueous fluid (connate waters?) mixture that migrated from the sedimentary source rock into the Jurassic host rocks where pyrite and pyrobitumen precipitated in the andesite. Late Cu-bearing hydrothermal fluids interacted with this pyrobitumen-pyrite assemblage to form Cu sulfides, either by replacement of pyrite or precipitation. We conclude that some of the S contained in pyrobitumen could have been released during interaction with the Cu-bearing hydrothermal fluid contributing, at least partially, to the S budget required for sulfide mineralization in the main ore stage. Our results provide evidence supporting pyrobitumen-fluid interaction as a key process in the formation of the Lorena deposit and possibly other stratabound Cu-(Ag) deposits in Chile.

* Corresponding author at: Department of Geology and Andean Geothermal Center of Excellence (CEGA), FCFM, Universidad de Chile, Plaza Ercilla 803, Santiago, Chile.
E-mail address: andrea.herazo@ug.uchile.cl (A. Herazo).

https://doi.org/10.1016/j.oregeorev.2020.103639
Received 19 March 2020; Received in revised form 27 May 2020; Accepted 7 June 2020
Available online 13 June 2020

1. Introduction

Over the past decades, several studies have recognized that organic matter can have a crucial role in the formation of mineral deposits (Mossman et al., 1993; Robb and Meyer, 1995; Large et al., 2011). The close spatial association between ore mineralization and solid oil residues or bitumen has been commonly interpreted to be either coincidental or to provide evidence for redox-induced ore precipitation by interaction of metal-bearing fluids with organic matter (Parnell, 1988; Anderson, 1991; Spirakis, 1996; Sun and Püttmann, 2000; Cuney, 2009; Pfaff et al., 2010; Large et al., 2011). However, recent studies have provided evidence that liquid hydrocarbons or crude oil can play a more active role during ore genesis by transporting metals and ligands from its source to the site of ore deposition (Migdisov et al., 2017; Saintilan et al., 2019). It is well known that trace metals (V, Ni, Zn, Au, U) and ligands (S, Cl, I) can be concentrated in different organic materials derived from sediments during diagenesis. These include liquid and solid hydrocarbons such as crude oil and (pyro)bitumen, respectively, in which reported U, V, Ni, Fe, Zn and Au contents can reach economic concentrations (Colombo and Sironi, 1961; Colombo et al., 1964; Hitchon et al., 1975; Jones, 1975; Ellrich et al., 1985; Mastalerz and Glikson, 2000; Lo Mónaco et al., 2007; Fuchs et al., 2016). Furthermore, recent experimental data have shown that Zn, Au and U can be solubilized in crude oils under different temperature conditions (Migdisov et al., 2017), and studies in Pb-Zn sediment-hosted deposits suggest that crude oil or petroleum could not only provide metals but also supply reduced sulfur for metal sulfide precipitation (e.g., Laisvall deposit, Sweden, (Saintilan et al., 2019). These investigations provided evidence of the potential role of liquid hydrocarbons in ore formation, highlighting that it could be more relevant than previously thought.

Despite these advances, two fundamental questions remain unanswered. The first relates to the relative timing of liquid hydrocarbon introduction into the ore system with respect to hydrothermal fluid circulation. This issue is critical in order to evaluate if the organic phase can act as a viable source of metals and ligands, or if it plays only a passive role as a reducing agent of dissolved species transported by the hydrothermal fluid. The second question deals with the absolute concentrations of trace metals that are present in liquid and solid hydrocarbons. Evidence is generally scarce and with the exception of a few studies (e.g., Jones, 1975; Ali et al., 1983; Wilson and Zentilli, 1999; Fuchs et al., 2016; Wu et al., 2020), the metal concentrations in organic phases remain mostly unconstrained. In addition, it is uncertain whether the organic phase retains its original metal load during interaction with hydrothermal ore fluids (Crede et al., 2019) or if hydrocarbons acquire metals as a result of this interaction. Within this perspective, hydrocarbons formed from a sedimentary rock could transport not only dissolved metals but also ligands such as sulfur (Lewan, 1984; Watkinson, 2007; Khuhawar et al., 2012), and later migrate through permeable rocks or favorable structural zones to shallower reservoir rocks where they can precipitate sulfide minerals. Alternatively, hydrocarbons could act as a geochemical trap for Cu-bearing aqueous hydrothermal fluids, triggering Cu sulfide precipitation as a result of changes in redox conditions.

The stratabound Cu-(Ag) deposits of northern and central Chile provide an ideal example to investigate some of the issues mentioned above. These deposits, also known as “Manto-type”, represent the third most important source of copper in Chile after porphyry Cu and iron oxide-copper-gold (IOCG) deposits, and can also contain economic levels of silver (Maksaev et al., 2007; Reich et al., 2010, 2013). Most importantly, several studies have recognized the association of Cu-(Fe) sulfides and sulfosalts with solid hydrocarbons or bitumen within “Manto-type” deposits of Cretaceous age in central Chile (Mayer et al., 1990; Zentilli et al., 1997; Wilson and Zentilli, 1999; Wilson et al., 2003a,b; Cisternas and Hermosilla, 2006; Rieger et al., 2008; Carrillo-Rosúa et al., 2014). These studies have shown that solid hydrocarbons, referred loosely as “organic matter”, “carbon” or “bitumen”, are morphologically and chemically complex structures.

Petroleum fluids are a mixture of organic molecules of different molar mass and structure that vary from a gaseous to liquid state (Tissot and Welte, 1984). Kerogen is the main precursor in petroleum generation and is defined as insoluble (in organic solvents) sedimentary organic matter derived from plants and other biomass (e.g., bacteria, animals). During early stages of burial, kerogen is subjected to microbial activity to form methane at temperatures between 10 °C up to 60–80 °C. At greater depths and temperatures (usually > 100 °C), thermal dissociation (“cracking”) and disproportionation leads to the formation of liquid hydrocarbons (i.e., crude oil) and thermal gas. Another precursor is soluble organic matter (bitumen). Bitumen is mainly generated from kerogen and includes oil, but also heavier, tar-like products. If this bitumen is thermally affected, it transforms into gas and a solid residue, ultimately methane and pyrobitumen (Gaupp et al., 2008). By focusing on the inorganic chemistry of pyrobitumen, we intend to obtain information that is essential to understand the role of hydrocarbons in the ore-forming process.

In this study, we present the results of a mineralogical and geochemical study of pyrobitumen from the Jurassic Lorena stratabound Cu-(Ag) deposit, Las Luces district, northern Chile. The presence of pyrobitumen has not been previously recognized in the Jurassic belt. Hence, its specific role in processes leading to Cu mineralization remains unaccounted. We combined detailed surface and drill core sample characterization and micro-textural observations with elemental data and chemical mapping of pyrobitumen obtained using electron microprobe and microscopic X-ray fluorescence analyses. In addition, we explored the speciation of sulfur in pyrobitumen using synchrotron-based spectroscopic techniques. The acquired data constrain the sources of metals and sulfur at Lorena and provide new insights into the role of hydrocarbons during the formation of stratabound Cu-(Ag) deposits in the Coastal Cordillera of northern Chile.

2. Geological background

2.1. Upper Jurassic and Lower Cretaceous stratabound Cu-(Ag) deposits

Stratabound or “Manto-type” Cu-(Ag) deposits occur along the Coastal Cordillera of northern and central Chile (Fig. 1), and are hosted by Upper Jurassic or Lower Cretaceous volcanic and volcano-sedimentary rocks. In the Coastal Cordillera of northern Chile, the deposits are spatially associated with the NS-trending Atacama Fault System (AFS), which played a fundamental role in the formation of the Jurassic-Cretaceous metallogenic belt (Barra et al., 2017 and references therein). Two groups of stratabound Cu-(Ag) deposits occur along the Coastal Cordillera of northern-central Chile. The first group in northern Chile (e.g., Mantos Blancos, Michilla, Buena Esperanza, Las Luces) is hosted by the Jurassic La Negra Formation, a 7000 m thick volcanic and volcanoclastic sequence. The second group of deposits, located in central Chile (e.g., El Soldado, Talcuna, Uchumi), is hosted by Lower Cretaceous volcanic and volcano-sedimentary rocks (Zentilli et al., 1997; Wilson and Zentilli, 1999; Maksaev et al., 2007; Kojima et al., 2009).

Sulfide mineralization in stratabound Cu-(Ag) deposits comprise mainly bornite, chalcocite, chalcopyrite, and minor pyrite, covellite and djurlerite (Espinoza et al., 1996; Kojima et al., 2009; Barra et al., 2017). Orebodies are structurally and stratigraphically controlled and are dominated by breccias, veins and stratiform lenses or “mantos”. Hydrothermal alteration is represented by selective sodic alteration of plagioclase, weak calcium metasomatism and abundant hematite. A more detailed description of both the Jurassic and Cretaceous belt can be found in (Maksaev et al., 2002; Maksaev et al., 2007; Kojima et al., 2009).

Deposits hosted by Lower Cretaceous volcanic rocks are unique due to their unusual association of Cu sulfides with migrated hydrocarbons hosted in lavas, subvolcanic intrusive bodies and pyroclastic units

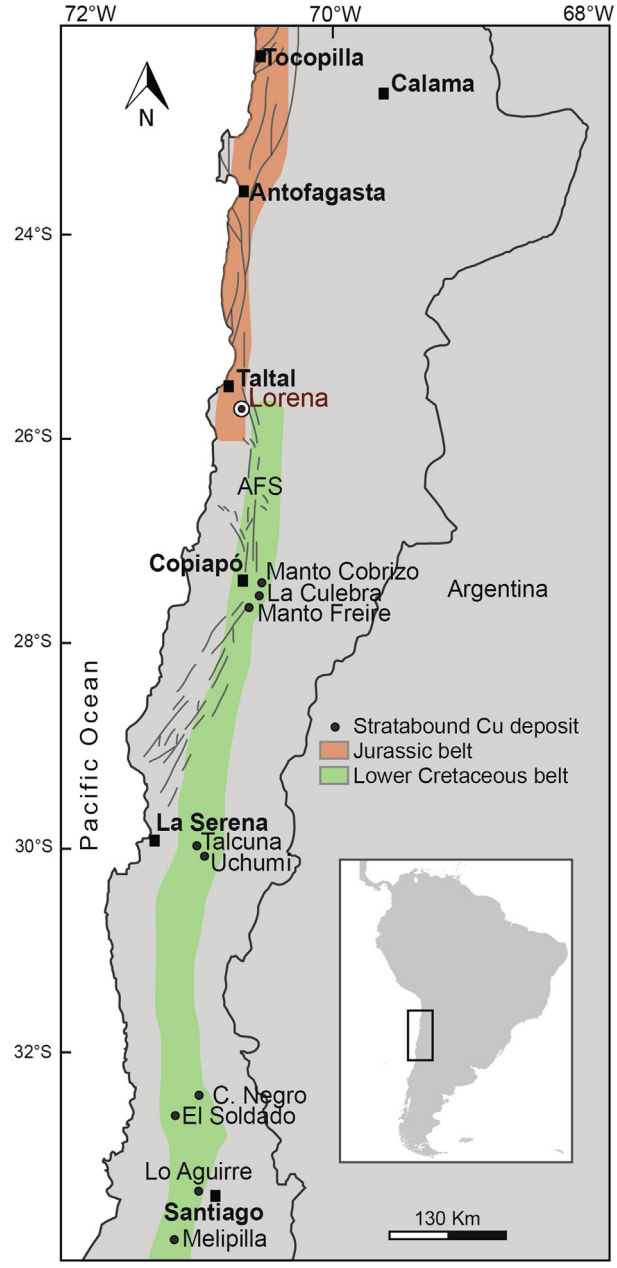

Fig. 1. Location of representative Jurassic and Cretaceous stratabound Cu-(Ag) deposits of the Coastal Cordillera of northern-central Chile. The extension of Jurassic and Lower Cretaceous belts and the NS-trending Atacama Fault System (AFS) are also shown.

(Mayer et al., 1990; Zentilli et al., 1994; Zentilli et al., 1997; Wilson and Zentilli, 1999; Boric et al., 2002; Haggan et al., 2003; Wilson et al., 2003a,b; Cucurella et al., 2005; Cisternas and Hermosilla, 2006; Wilson and Zentilli, 2006; Rieger et al., 2008; Carrillo-Rosúa et al., 2014). In these deposits, hydrocarbons occur as (pyro)bitumen. The most notable example within this metallogenic belt is the El Soldado deposit in central Chile (Wilson and Zentilli, 1999; Wilson et al., 2003b), where pyrobitumen is found in close association with Cu minerals. Other pyrobitumen-bearing deposits of inferred Cretaceous age have been reported near the cities of Copiapó (e.g., Manto Cobrizo, La Culebra; (Cisternas and Hermosilla, 2006), La Serena (e.g., Talcuna, Uchumi; (Wilson and Zentilli, 2006), and Santiago (e.g., Melipilla-Naltahua; (Carrillo-Rosúa et al., 2014), Lo Aguirre; (Saric et al., 2003) (Fig. 1). The reconnaissance of an intimate spatial association of pyrobitumen and Cu mineralization has been considered by the cited authors as a key factor in the genesis of some of the Lower Cretaceous stratabound Cu-(Ag) deposits. In contrast, no pyrobitumen has been reported in the deposits hosted by the Jurassic La Negra Formation in the Coastal Cordillera of northern Chile.

2.2. The Lorena stratabound Cu-(Ag) deposit

The Lorena deposit (~200,000 metric tons @ ~1.5% Cu sulfide; ~300,000 metric tons @ 0.9% Cu oxide) forms part of the Las Luces district, near Taltal in the Antofagasta region of northern Chile (Fig. 2A). The Las Luces deposit, as a reference, has current resources estimated at 2.3 Mt with 1.11% Cu (Zamora, 2011). In the Las Luces district, the volcanic rocks of La Negra Formation are represented by basaltic andesite and andesite lava flows, volcanoclastic layers and minor volcanic breccias (Fig. 2B). The sequence forms a monocline fold with a NE trend and variable dip between 12° – 25° SE (Zamora, 2011). Jurassic volcanic rocks from the Posada de los Hidalgos Formation are present in the southwest part of the study area. Older Paleozoic metasedimentary rocks of the Las Tórtolas Formation and Early Jurassic (Hettangian to Sinemurian) marine sedimentary rocks from the Pan de Azúcar Formation (Naranjo, 1978; Ulriksen, 1979; Naranjo and Puig, 1984) outcrop in the western part of the district (Fig. 2B). La Negra Formation is intruded by several mafic to felsic stocks and dikes of Early Jurassic to Lower Cretaceous age that vary in composition from gabbro to diorite and granodiorite, with scarce tonalite and granites (e.g., Matancilla Plutonic Group, (Naranjo and Puig, 1984). Geochronological data indicate that the emplacement of the plutonic bodies occurred mainly during two periods, i.e., 190 – 173 Ma and 160 – 142 Ma (Pichowiak et al., 1990; Boric et al., 1990; Scheuber and Gonzalez, 1999; Oliveros et al., 2006, 2008). La Negra Formation overlies marine sediments, continental deposits or metapelitic rocks of the Cifuncho Formation (García, 1967; Pichowiak et al., 1990) (Fig. 2B). Overlying the volcanic rocks of La Negra is the Lower Cretaceous Aeropuerto Formation, which comprises porphyritic andesites intercalated with andesitic tuffs and breccias, conglomerates, sandstones and fossiliferous limestones (Naranjo and Puig, 1984; Boric et al., 1990). In the study area, the Aeropuerto Formation is completely covered by the unconsolidated Atacama Gravels of Oligocene to Miocene age (Fig. 2B).

The basaltic andesite to andesite rocks of the La Negra Formation, which host the Cu mineralization at Lorena, exhibit mainly a porphyritic texture with large plagioclase and pyroxene phenocrysts (~1 to 2 cm). Amygdaloidal and aphanitic textures are also recognized. The matrix is mostly intersectal with plagioclase and pyroxene microliths, and disseminated magnetite. The deposit is both structurally and stratigraphically controlled, and the sulfide-pyrobitumen mineralization is mostly found in breccias and “mantos”. The main structural feature in the deposit is a NW-trending fault. Near this fault, the andesite is affected by pervasive albitization, with pyrobitumen within the albite-chlorite-hematite matrix. Additionally, post-mineralization mafic sills of diorite-gabbroic composition cross-cut the volcanic host rock sequence.

At Lorena, the Cu-(Fe) sulfide mineralization occurs in breccias, fractures, veins or vesicle-fillings (Fig. 3A-D). The ore mineral assemblage comprises chalcocite-bornite with minor chalcopyrite, pyrite and late digenite, covellite, chrysocolla and malachite. Pyrobitumen is observed filling mm- to cm-sized vesicles (Fig. 3A, B), and is intimately associated with Cu sulfides (Fig. 3B, C) and very low-grade metamorphic mineral assemblages (zeolite-prehnite-pumpellyite). Pyrobitumen also occurs as mm- to cm-sized granular aggregates and fracture fillings (Fig. 3C, D). Moderate calcic and sodic metasomatism (chlorite, epidote and albite) is also recognized and calcite is present in late-stage veinlets. A detailed description of the mineral paragenesis is presented in the Results section.

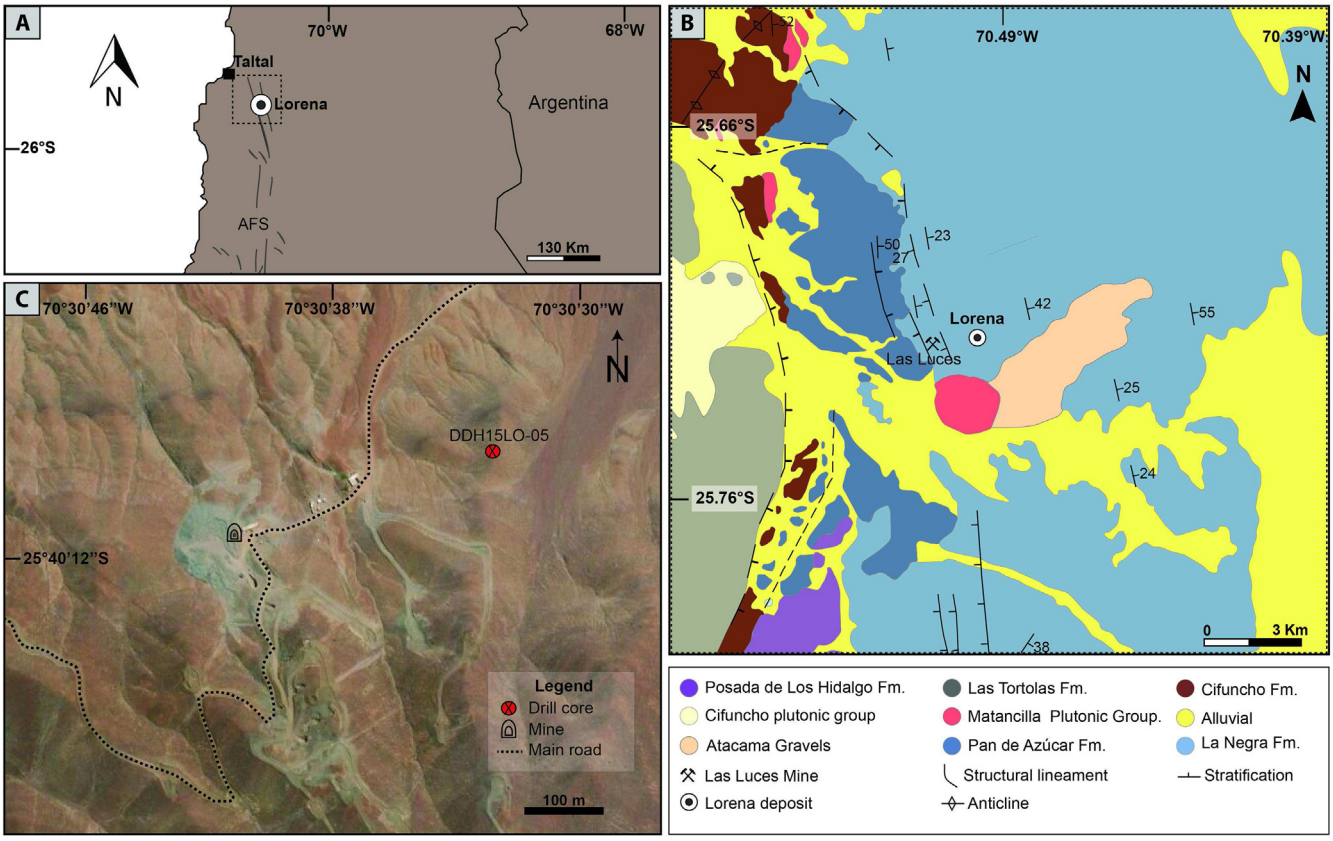

Fig. 2. A) Location of the Lorena deposit, Las Luces district. B) Geologic map of the Las Luces district (modified from (Detlef, 2002). C) Satellite image of the Lorena (underground) mine showing the location of the sub-vertical DDH15LO-05 drill hole collar.

3. Samples and methods

One representative ~300 m long sub-vertical drill core from the Lorena deposit was selected for this study (drill core DDH15LO-05, 312 m; Fig. 2C). Thirty-four samples were obtained from this drill core, and twenty-six polished thin sections were selected for optical inspection using reflected and transmitted light microscopy. Sample selection was focused on the presence of pyrobitumen associated with sulfides. Characterization of the pyrobitumen-bearing sulfide assemblages at Lorena was achieved using a combination of imaging, microanalytical and spectroscopic techniques.

3.1. SEM, FE-SEM and EMPA methods

Scanning electron microscopy (SEM) observations were performed at the Andean Geothermal Center of Excellence (CEGA), Universidad de Chile, Santiago, Chile using a FEI Quanta 250 SEM equipped with secondary electron (SE), backscattered electron (BSE) and X-ray energy-dispersive spectrometry (EDS) detectors. The analytical parameters were: accelerating voltage of 15–20 kV, filament current ~80 μA, beam intensity of 1 nA, takeoff angle ~35°, a spot size of 4–5 μm in diameter, and a working distance of ~10 mm. The INCA software was used for measurements and data processing. Semi-quantitative EDS analyses were used to constrain major elements in individual mineral phases and pyrobitumen. The EDS operating conditions were 20 keV, a spot size of 1–3 μm and a working distance of 10–18 mm. High-resolution imaging of micro- to nano-sized inclusions in sulfides and pyrobitumen was achieved using field-emission scanning electron microscopy (FE-SEM). Observations were performed using a FEI Quanta 250 FEG instrument at the Center for Research in Nanotechnology and Advanced Materials (CIEN) at the Pontificia Universidad Católica de Chile, Santiago, Chile. The FE-SEM is equipped with in-column detector (ICD) for SE and BSE, and an EDS detector. Operating conditions included an accelerating voltage of 20 kV, the beam spot size was ~4 μm in diameter, takeoff angle ~35 to 37°, live time was 45 s, and a working distance of ~10 mm.

The chemical composition of minor elements in pyrobitumen was determined in two analytical sessions performed at different electron microprobe laboratories. The first session was carried out using a JEOL JXA-8500F microprobe at the Peter Hooper GeoAnalytical Laboratory, Washington State University, Pullman, USA, and the second by using a JEOL JXA-8230 microprobe at the LAMARX Laboratory of the Universidad Nacional de Córdoba, Argentina. The same operating conditions were set in both instruments and included an accelerating voltage of 20 kV, a beam current of 10 nA and a 10 μm beam. Evidence of beam damage of pyrobitumen grains was checked systematically between analyses. No pyrobitumen disturbance due to electron beam irradiation was noted. Calibration was achieved by using natural and synthetic standards and included YVO_4 (for V), $FeCr_2O_4$ (for Cr), FeS_2 (for Fe), Co^0 (for Co), $(Ni,Fe)_9S_8$ for (Ni), FeAsS (for S and As), Sb_2S_3 (for Sb), AgI (for I), KCL (for Cl), Ag^0 (for Ag), Au^0 (for Au) and U_3O_8 (for U). Counting time (peak) was 10 s for Fe Kα, Ni Kα, Cu Kα, S Kα, Cl Kα; 15 s for V Kα, Cr Kα, Co Kα, U Kα 20 s for Ag Lα, 25 s for I Lα, 30 s for Sb Lα, Au Mα, and 60 s for Sb Lα. The half (peak) counting time was used for total background readings. Mean detection limits ranged from 0.01 to 0.03 wt% for most analyzed elements.

3.2. XRF elemental mapping

Micro X-ray fluorescence (μ-XRF) elemental mapping of pyrobitumen-bearing samples was performed at CSIRO Mineral Resources, Perth, Australia using a Bruker Tornado XRF desktop instrument equipped with a rhodium target X-ray tube operating at 50 kV and 500 nA without filters and an XFlash® silicon drift X-ray detector. Beam

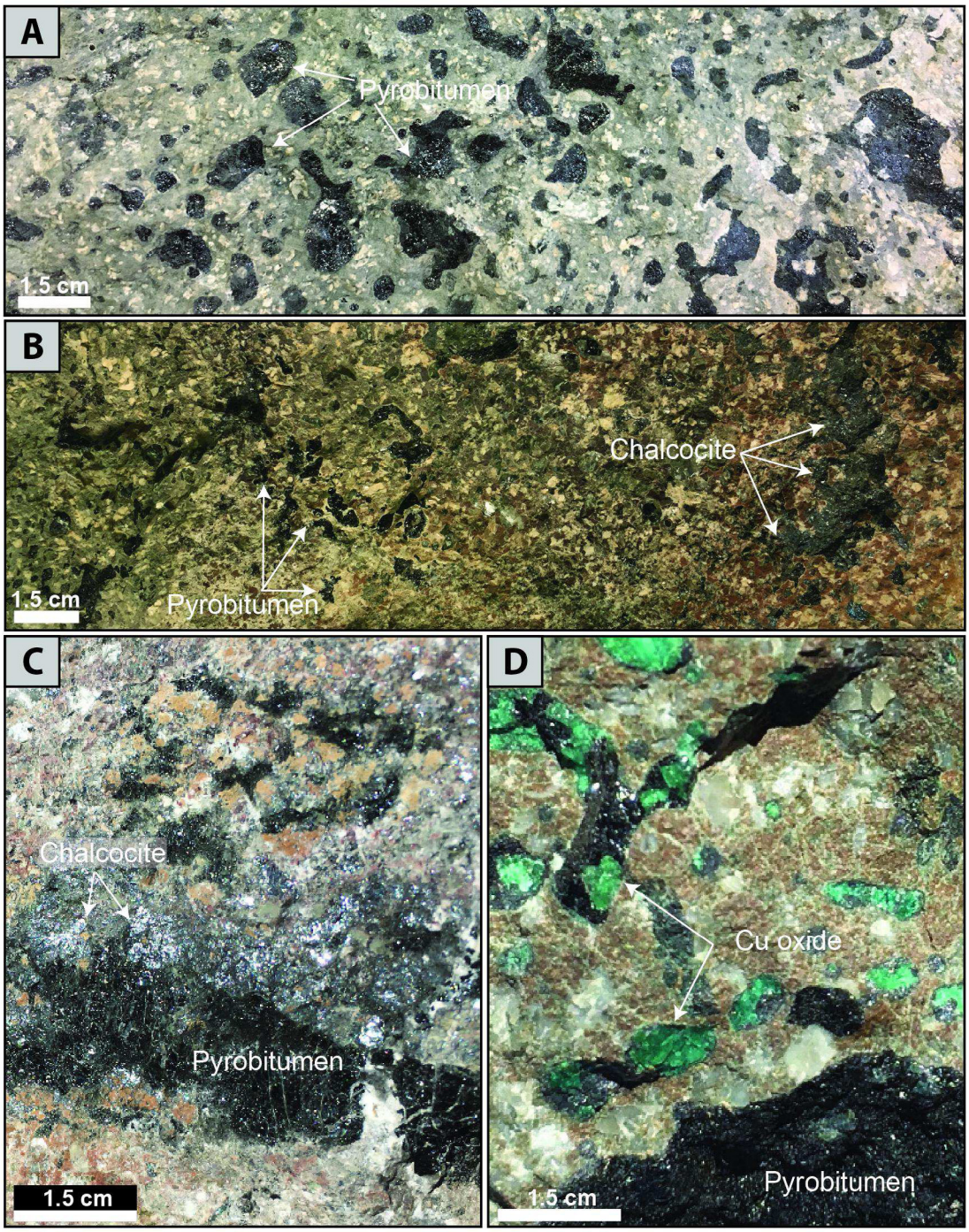

Fig. 3. Representative pyrobitumen-bearing andesitic host rock samples from the Lorena deposit. A) and B) Pyrobitumen filling vesicles has a black color, glassy luster and conchoidal fracture. C) Pyrobitumen associated with hypogene chalcocite. D) Pyrobitumen in contact with Cu oxides formed by in-situ oxidation of hypogene sulfides.

diameter and point spacing of 40 μm was used for optimal map resolution, with dwell times varying from 3 to 10 ms depending on sample size. The elemental maps allowed visualization of the spatial variations in relative abundances of major and a few minor elements (S, Fe, Cu and V).

Synchrotron X-ray fluorescence (S-XRF) mapping of selected pyrobitumen grains was performed at the XRF beamline of the Brazilian Synchrotron Light Laboratory (LNLS), Campinas, Brazil. The XRF source is a 1.67 T bending magnet. The beamline has a flux density of 2×10^8 photons/s/mm^2/100 mA, and is equipped to cover an energy range of 5–20 keV, producing a highly focused microbeam of 22×12 μm. The excitation of the samples deposited on Si (1 1 1) layers was performed using synchrotron radiation of a beam operating at 16.5 keV. The fluorescence radiation was recorded by a Si(Li) detector with energy resolution of 165 eV at 5.9 keV, and the detector was placed at a 90° angle from the incident beam (Pérez et al., 1999). The irradiation time was 100 s. All measurements were performed in duplicate. Filters were used to attenuate effects of the matrix, atmosphere, detector and beam. Calibration was perfomed by using the NIST 612 reference material, which contains four major components (SiO_2, CaO, Na_2O, Al_2O_3) and twenty-one elements (Co, Cu, Fe, Mn, Ni, Sr, Ti, K, Rb, Ba, Dy, Er, Nd, Ag, Ce, Eu, Gd, La, Pb, U, Yb). The standard was

measured for 100 s. The obtained X-ray spectra were processed using the PyMca software in order to obtain the X-ray intensities for each element and the associated uncertainty.

3.3. Sulfur X-ray absorption near edge structure (XANES) spectroscopy

X-ray absorption near edge structure (XANES) was used to obtain chemical information of sulfur speciation in pyrobitumen (e.g., Pomerantz et al., 2014). Sulfur has six oxidation states that can be distinguished as peaks in the absorption spectrum within an X-ray energy window between 2470 and 2482 eV. In-situ XANES measurements of sulfur K-edge in pyrobitumen were recorded in fluorescence-yield mode at the SXS line of the Brazilian Synchrotron Light Laboratory (LNLS) in Campinas, Brazil. The beamline uses a high-flux beam ($\geq 4.5 \times 10^{11}$ photons/s/mm^2/100 mA) that is equipped to achieve a focused 200 μm beam using toroidal mirrors, and can cover an energy range between 1 and 5 keV. Spectra were collected from 2430 to 2600 eV, with steps sizes of 0.2 eV at the S K-edge and 1 and 3 eV for the pre-and post-edge regions, using 1 s scan duration per energy step. The standard used for calibration was CaP (Bayovar). Chalcopyrite ($CuFeS_2$), sodium sulfite (Na_2SO_3) and gypsum ($CaSO_4$) powders were used as inorganic standards. These were diluted in boron nitrate at approximately $<$ 1 wt% to minimize self-absorption. The diluted standards were transferred into a cup and sealed with 7.5 μm thick Kapton film before analysis in the X-ray source. XANES measurements were performed on thin sections with large pyrobitumen grains (mm-cm). Only isolated pyrobitumen grains were analyzed to avoid contamination by sulfide minerals. The spectra acquisition was carried out with the Amptek DPPMCA software. The data were analyzed by fitting the measured spectra to a linear combination of the model compounds and compared to sulfur K-edge XANES spectra for sulfur standards (Bolin et al., 2016; Annex Fig. 1).

4. Results

4.1. Variations with depth

Mineralization at the Lorena deposit comprises stratiform lenses ("mantos"), breccias, veins and disseminations hosted in basaltic andesite to andesitic rocks of the La Negra Formation (Figs. 3 and 4).

Drill core DDH15LO-05 shows that the orebodies are mineralized layers or "mantos" interspersed with unaltered or "fresh" rock (Fig. 4). Based on lithological and mineralogical characteristics, the investigated drill core was divided into three main sections, i.e., shallow (0–98.6 m), intermediate (~98.6 to 167 m), and deep (167–312 m), where different pyrobitumen types were identified: globular or rounded pyrobitumen (OM1), pyrobitumen inclusions within sulfides (OM2) and angular or sharp-edged pyrobitumen (OM3). The shallow or upper section is dominated by afanitic andesite and hydrothermal breccias (Fig. 4A-B) with minor chrysocolla. No pyrobitumen or hypogene sulfide mineralization were observed in this section.

The middle section (~98.6 to 167 m) is characterized by a transition from the shallow aphanitic andesite to a vesicular and porphyric andesite texture with sulfide mineralization. Mineralization is spread along this section and comprises pyrite, chalcopyrite as well as bornite with abundant chalcocite and minor covellite-digenite. The section is cross-cut by a barren microdiorite dike composed of abundant pyroxene and plagioclase. Pyrobitumen grains, which occur throughout this section (starting at ~98.6 m), range in size from a few tens of micrometers to a few centimeters. It is observed within the calcite/metamorphic minerals matrix, filling vesicles and fractures (Fig. 4C). Pyrobitumen in this section displays two distinct textures: globular (or rounded), and angular (i.e., sharp-edged grains). Globular pyrobitumen (OM1) is dominant and occurs as disseminated, drop-shaped vesicle fillings of approximately 1–5 mm in size (Fig. 4D), although in some cases pyrobitumen fillings can reach cm-sizes (e.g., Fig. 3A). Globular pyrobitumen (OM1) is related to albite, calcite and minor chlorite in vesicles. Angular pyrobitumen (OM3), on the other hand, is mostly restricted to fractures where it is intimately associated with sulfides (pyrite, chalcopyrite and chalcocite) and magnetite (Fig. 4E, F).

The deep or lower section (~167 – 312 m) corresponds to the main part of the deposit. The host rock is a vesicular andesite with a porphyritic texture comprising > 15% of plagioclase and minor pyroxenes. Sulfide minerals include pyrite, chalcopyrite and abundant chalcocite, which occur filling fractures, veins or vesicles. The highest Cu grades are found in breccias or near structures (mainly faults or fractures). Sulfides are associated with pyrobitumen, and usually form mineralized "mantos" up to ~15 m thick. Angular pyrobitumen (OM3) is the dominant textural type of pyrobitumen in this section and is often observed filling the center and/or coating the walls of large vesicles (Fig. 4E, F). Pyrobitumen inclusions within sulfides (OM2) are observed in this section, and correspond to micrometer- and nanometer-sized pyrobitumen droplets encapsulated within pyrite and chalcocite (see Section 4.3). Globular pyrobitumen (OM1) is also present as mm- to cm-sized aggregates, filling vesicles or fractures. Iron and Fe-Cu-bearing mineral inclusions occur within pyrobitumen, particularly at grain rims or filling both fractures and vesicles. Pyrobitumen grains (OM1 and OM3) are cross-cut by calcite veinlets.

4.2. Hydrothermal alteration and mineralization

The dominant hydrothermal alteration type in the deposit is albitization with minor epidote, sericite, chlorite and abundant calcite (Fig. 5). Albitization is observed as a widespread pre-ore alteration event that affected the andesite host rock and locally, the breccia matrix. Albite occurs replacing primary plagioclase laths (Fig. 5A, B, E). Albitized plagioclase can be further altered to sericite (Fig. 5B). Chlorite was recognized replacing pyroxene phenocrysts. It was also observed associated with prehnite-pumpellyite-pyrobitumen and calcite, filling vesicles, fractures and veinlets (Fig. 5C, D). Zeolites, prehnite-pumpellyite, chlorite, calcite and minor chalcedony, as well as pyrobitumen, are found filling vesicles and in the breccia matrix. Calcite is dominant over chlorite and two forms were identified, i.e., small calcite crystals with chlorite in veinlets and large calcite grains filling vesicles (Fig. 5E, F).

Pyrite is widespread and occurs mostly as small grains intimately associated with pyrobitumen (OM1) in zones with no Cu mineralization. Pyrite grains occur mainly as isolated or aggregates of euhedral crystals and rosette-like spherules (Fig. 6A-E). Pyrobitumen occurs mainly as isolated aggregates, filling vesicles and often with globular shape (Fig. 4C, D). The most distinctive feature of the pre-ore mineralization is the abundant presence of pyrobitumen and euhedral pyrite (Fig. 6A).

In the upper section of the drill core, pyrite is scarce, occurring mostly in the intermediate to deep zones (> 98.6 m depth). As mentioned previously, pyrite is intimately associated with globular pyrobitumen (OM1), and occurs as disseminated euhedral to anhedral grains in the host rocks or filling vesicles (Fig. 7A, B). A sharp increase in pyrite abundance was recognized at ~289.05 m in the drill core. Overall, two main textural types of pyrite were identified: 1) Euhedral to subhedral grains (Pyrite I) with occasional cubic and pyritohedral shapes ranging in size between 80 and 900 μm, but occasionally reaching up to 1.5 mm (Fig. 7A). These crystals display abundant fractures and minor magnetite inclusions. Aggregates of pyrite grains can form rosette-spherules (Pyrite II) textures (e.g., Fig. 7B). These aggregates grains display sharp, irregular rims with some pyrobitumen in the center of the crystals. In addition, abundant fractures have affected some of these grains resulting in a puzzle-like texture. Angular pyrobitumen (OM3) can be observed in some of these fractures.

The main Cu ore phases correspond to chalcocite, bornite and chalcopyrite (Fig. 6F). Chalcocite is the dominant Cu sulfide, and occurs as disseminated aggregates and filling fractures and is also intimately

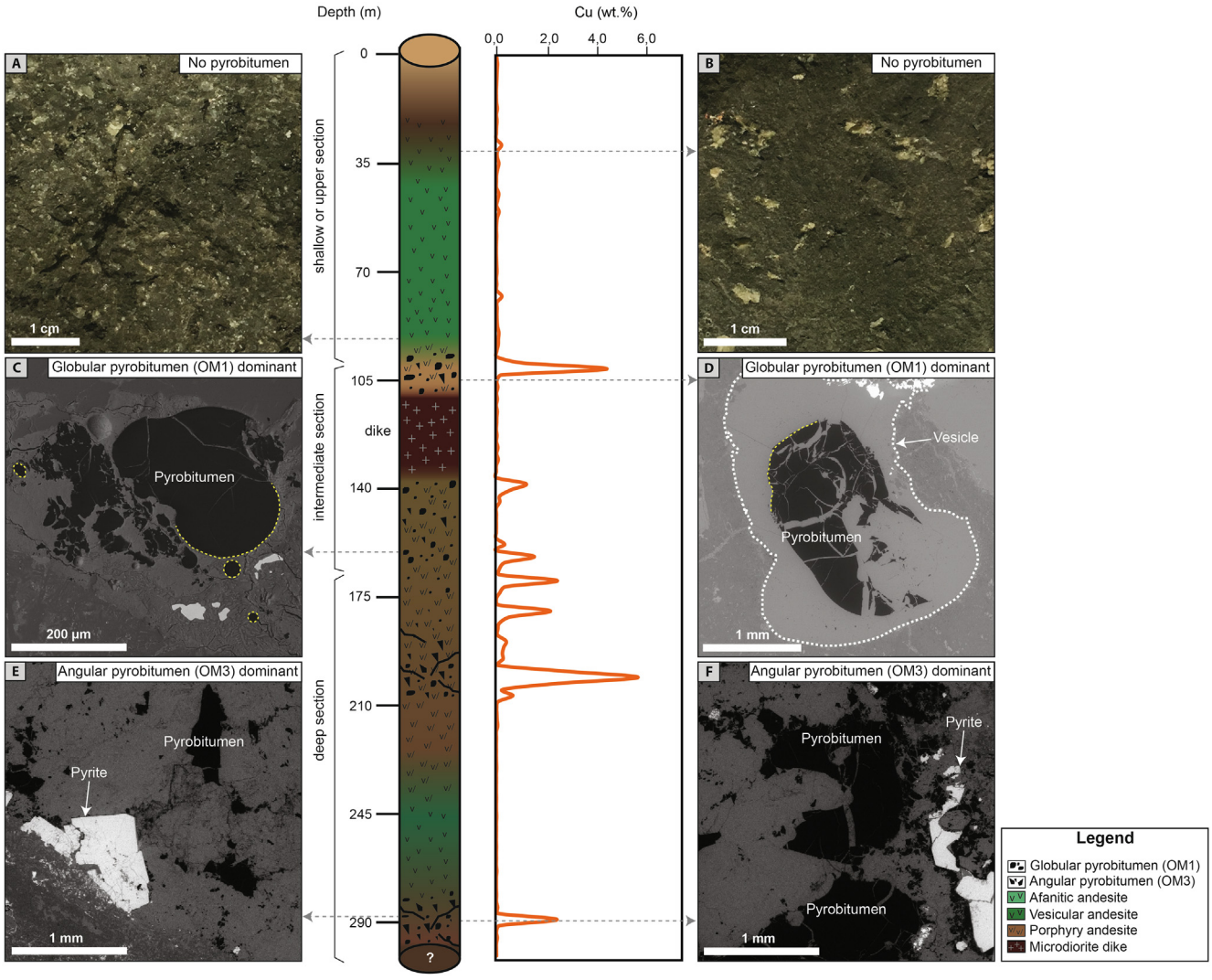

Fig. 4. Schematic illustration of drill core DDH15LO-05 from the Lorena deposit showing lithological variations (center) and images of representative samples along the drill core. The orange line indicates the average Cu grade from the top to the bottom of the drill core. A) Andesite with ~5 to 30 modal percentage of plagioclase phenocrysts. B) Afanitic andesite with scarce plagioclase phenocrysts (< 5 modal percentage). C-D) Backscattered electron (BSE) images of globular pyrobitumen filling a vesicle in a sample from the intermediate section. E-F) Backscattered electron (BSE) images of angular pyrobitumen. This textural type is dominant in the deep zone. Angular pyrobitumen grains vary in size and is commonly observed in brecciated zones.

associated with pyrobitumen (Fig. 3B, C; Fig. 6G, H). Chalcocite also occurs filling veinlets and within amygdales of the volcanic host rock, which are elongated and rounded, with sinuous, sharp edges, forming aggregates reaching up to 1.5 mm in diameter. Disseminated grains of chalcocite reach up to 250 µ m, and to a lesser extent as a replacement mineral of bornite. In the analyzed samples, chalcocite was observed in association with pyrobitumen, calcite, and prehnite-pumpellyite at depth (> 105 m). Chalcocite grains usually occur with angular fragments of pyrobitumen (OM3) (Fig. 3C). Hematite is associated with chalcocite and can also replace magnetite in the upper part of the deposit. Late-stage (supergene) assemblages include covellite, digenite, djurleite, chrysocolla and malachite, generally replacing chalcopyrite and chalcocite (e.g., Fig. 3D, 6F, G).

4.3. Pyrobitumen inclusions in pyrite and chalcocite

Petrographic observations at Lorena show the occurrence of drop-like pyrobitumen inclusions within pyrite and chalcocite (OM2). For example, a distinct feature of pyrite grains from the deep section of the drill core is the ubiquitous presence of micrometer- and nanometer-sized pyrobitumen inclusions. These inclusions consist mainly of droplet-shaped pyrobitumen grains (Fig. 8). They occur in pyrite crystals as randomly oriented inclusions (Fig. 8A-C), following crystallographic planes and growth zones (Fig. 8B-D), and also near the grain rims (Fig. 8A). Detailed observations using a high-resolution FE-SEM show that the pyrobitumen inclusions are up to 600 nm in size (Fig. 9). In addition to the linear alignment of pyrobitumen inclusions (Fig. 8), isolated pyrobitumen micro-inclusions were observed in the cores of pyrite grains (Fig. 9D-E). FE-SEM-EDS revealed the presence of Al and Si rich nanoparticles within these pyrobitumen micro-inclusions (Fig. 9F). These nanoparticles were usually observed in the center or at the rims of pyrobitumen droplets.

Most importantly, droplet-shaped inclusions of pyrobitumen of variable size (~700 nm to 20 µm) were also recognized randomly distributed within some chalcocite grains (Fig. 6H, 10). These bitumen inclusion-bearing chalcocite crystals, when present, are commonly associated with larger pyrobitumen grains.

4.4. Elemental composition and pyrobitumen textures

Electron microprobe analyses of pyrobitumen from the Lorena deposit are reported in Appendix A. Analyses were performed on clean

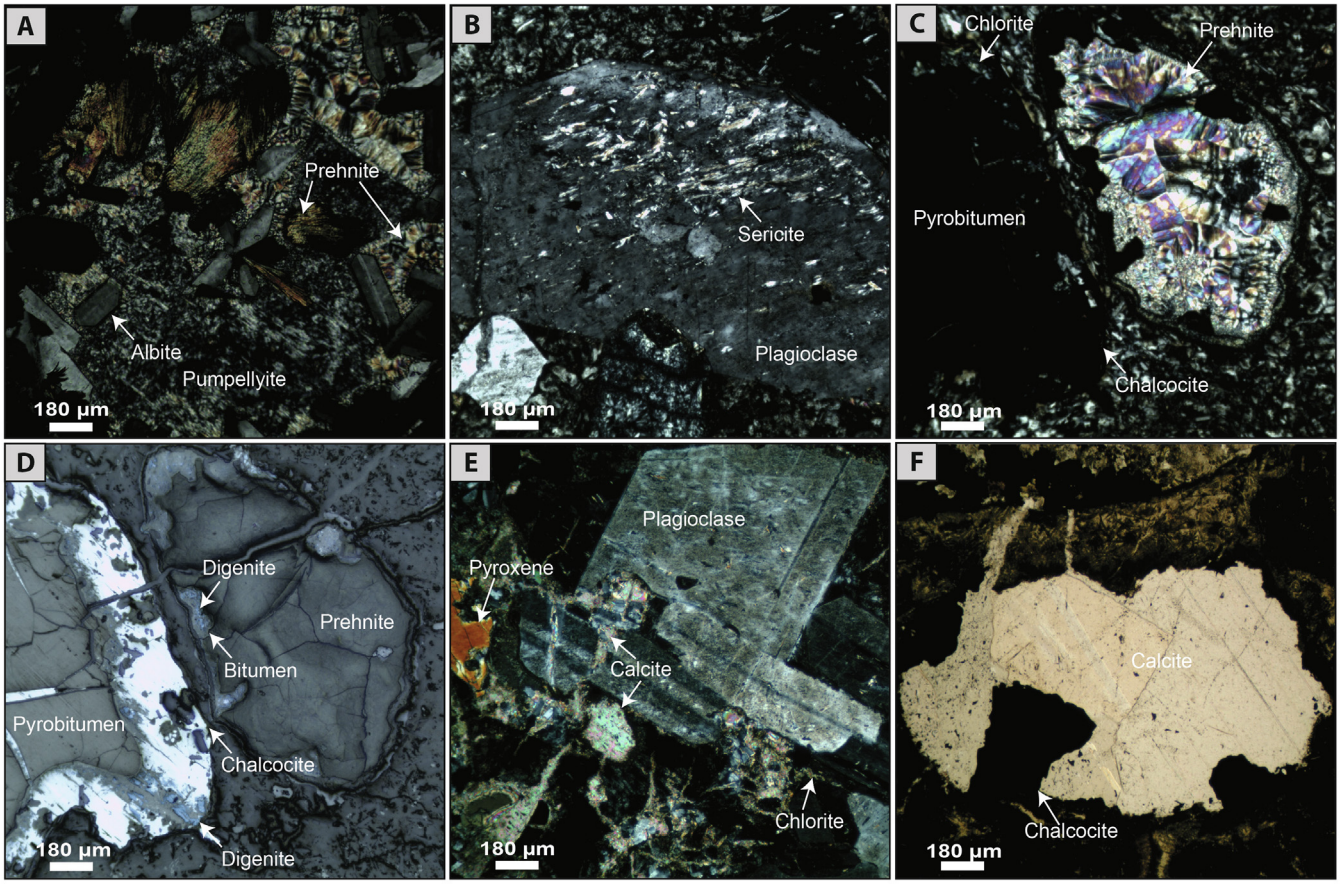

Fig. 5. Transmitted and reflected polarized light microscopy photomicrographs of representative alteration minerals at Lorena. A) Prehnite and pumpellyite in vesicles with albite microcrysts. B) Albitized plagioclase with minor sericite. C) Vesicle infilled with prehnite with minor pyrobitumen at the edges. D) Reflected light image of (C) where copper sulfides (chalcocite and digenite) are observed in close association with pyrobitumen. E) Albitized plagioclase phenocrysts cross-cut by thin calcite veinlets. F) Calcite and chalcocite amygdale in volcanic host rock.

pyrobitumen areas with no visible mineral inclusions. Iron, Cu, S, Cl, Ag, Au, U, V, Co, As, Cr, Ni and Sb were measured. It is important to note that only globular (OM1) and angular (OM3) bitumen grains were analyzed. The smaller bitumen inclusions in the sulfides (OM2) could not be analyzed due to their small size (< 1 µm), usually below the spatial resolution of the electron probe (and the other micro-analytical techniques used here, i.e., XRF and XANES) (see Methods section).

A statistical summary of elements with concentrations above the

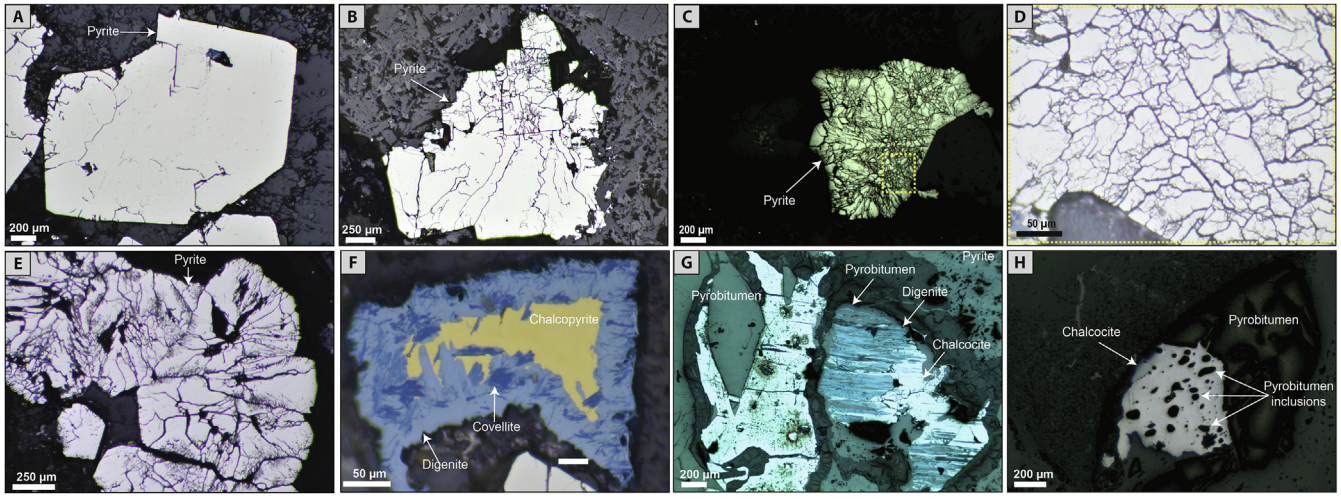

Fig. 6. Reflected polarized light microscopy images of pre-ore and ore stage assemblages from the Lorena deposit. A) Euhedral pyrite (Pyrite I) from the pre-ore stage, B) Pyrite overgrowths from on pre-existing euhedral pyrite core, forming elongated and sub-rounded clusters. C) Rosette-shaped pyrite aggregates (Pyrite II). D) shows the magnified image of the yellow rectangle in (C), highlighting the finer structures of the pyrite aggregates. E) Set of rosette-shaped pyrite aggregates. F) Chalcopyrite grain replaced by digenite and covellite. G) Pyrobitumen/chalcocite association replaced by late digenite. H) Droplet-shaped, micrometer-sized pyrobitumen inclusions within chalcocite.

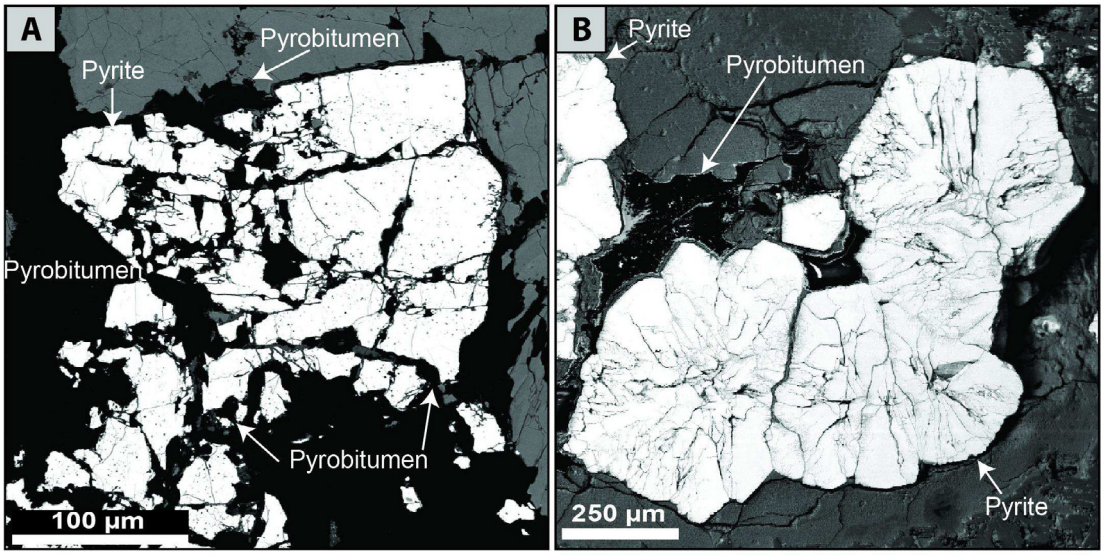

Fig. 7. Backscattered electron (BSE) images showing pyrobitumen in association with pyrite. (A) Subhedral pyrite grains with pyrobitumen interspersed or filling fractures. B) Rosette-shaped pyrite, showing pyrobitumen inclusions and in simple contact with pyrobitumen grains.

detection limit is presented in Fig. 11. All elemental data are displayed in Annex Fig. 2, including below detection values. No significant chemical differences were observed between globular (OM1) and angular (OM3) pyrobitumens. Hence, and for the sake of simplicity, EMPA data are plotted as a whole in Fig. 11. Pyrobitumen at Lorena displays high concentrations in Fe, Cu, S and Cl, reaching maximum concentrations in the 1000 ppm range. Concentrations of the aforementioned elements are variable, spanning from 100′s to 1000′s of ppm. Sulfur was detected in almost all analyses revealing some of the highest concentrations (up to 0.43 wt%), and also showing the lowest variability. Vanadium, Co and As were detected in about 25% of the analyses with mean concentrations of 200, 290 and 230 ppm, respectively. Chromium, Ni, Sb, Ag were detected only in a few pyrobitumen grains with concentrations $<$ 400 ppm and U was only reported in one spot with a concentration of 200 ppm (Appendix A). Silver was detected in only two spots with a concentration of 300 ppm and Au was detected in 15 spots reaching up to 600 ppm with a median concentration of 400 ppm (Fig. 11).

Fig. 12 depicts the above-detection EMPA data of pyrobitumen, plotted as a function of depth (all elemental data are included in Annex Fig. 3). Pyrobitumen at Lorena show some chemical variations with depth. In particular, Fe, Cu and Cl concentrations increase progressively as a function of depth, whereas S shows moderate variation, ranging from an average of 0.35 wt% in the shallow-intermediate section to 0.28 wt% in the deep zone (Fig. 12). In the intermediate section, average concentrations of Cu, Fe and Cl are 0.13, 0.09 and 0.01 wt%, respectively. Pyrobitumen grains located at depth, when compared to those in the upper section, display a larger compositional variability with average Fe, Cu and Cl concentrations of 0.14, 0.24 and 0.17 wt%, respectively.

4.5. Pyrobitumen XRF maps

Elemental maps at the mm to µm scale of selected pyrobitumen grains (OM1 and OM3) from Lorena are presented in Fig. 13. Desktop µ-XRF (Fig. 13B-J) and synchrotron XRF (Fig. 13L-R) maps were obtained for pyrobitumen from intermediate and deep sections of the studied drill core.

Elemental maps of globular-rounded (OM1) and angular pyrobitumen (OM3) from the intermediate section reveal that sulfur is homogenously distributed within the grains (Fig. 13B, G). Copper concentrations were detected in fractures around pyrobitumen, and only sparse copper pixels were observed within pyrobitumen (e.g., Fig. 13H). Vanadium was also recognized in pyrobitumen, in agreement with EMPA data, although the highest signal intensity was observed in the host rock (Fig. 13D, I).

Synchrotron XRF (S-XRF) maps show that sulfur is distributed within pyrobitumen grains in moderate to highly mineralized samples from the intermediate section, in good agreement with desktop µ-XRF maps. Furthermore, and due to the higher resolution of the technique, S-XRF maps show lower S concentrations towards pyrobitumen grain rims in samples from deep section (Fig. 13M). On most maps, higher Ca concentration zones around pyrobitumen grains reflect the presence of calcite (Fig. 13C, L). Other elements, such as As, Cr, Ag and Cu, were only randomly observed in maps (Fig. 13N-Q) and are usually detected along fractures (e.g., Cu, Fig. 13H, J). EMPA-WDS X-ray maps provide additional spatial information about the Cu distribution in pyrobitumen at the grain scale. These images show that the highest Cu concentrations are observed in the host rock matrix surrounding pyrobitumen grains (Fig. 14).

4.6. Sulfur XANES data

Sulfur XANES measurements in pyrobitumen were performed in two samples from the deep section. These pyrobitumen-bearing samples were selected considering the size (mm to cm) of the pyrobitumen grains and also the absence of Cu-(Fe) sulfides. Several spots were analyzed and merged to achieve average oxidation states for sulfur within each sample (see Evans et al., 2014; Konecke et al., 2017). Two different spectral types were identified (Fig. 15). Globular pyrobitumen (OM1) in sample LO-24-SP1 shows peaks at 2470 eV and 2482 eV that correspond to elemental sulfur (S^0) and sulfate (S^{6+}) species, respectively. Pyrobitumen in brecciated areas (OM3) in sample LO-24-SP4 exhibits an average sulfur K-edge sharp peak of S^{2-} (2471 eV) with a minor peak at 2473 eV, and a S^{2+} broad peak (2478 eV) (Fig. 15). These peaks correspond primarily to two sulfur species, i.e., thiophene (2471 eV) and sulfone (2478 eV).

5. Discussion

5.1. Paragenetic sequence and ore-forming processes

Sulfide mineralization at Lorena is similar to that described at the Las Luces deposit, where main hypogene and late supergene

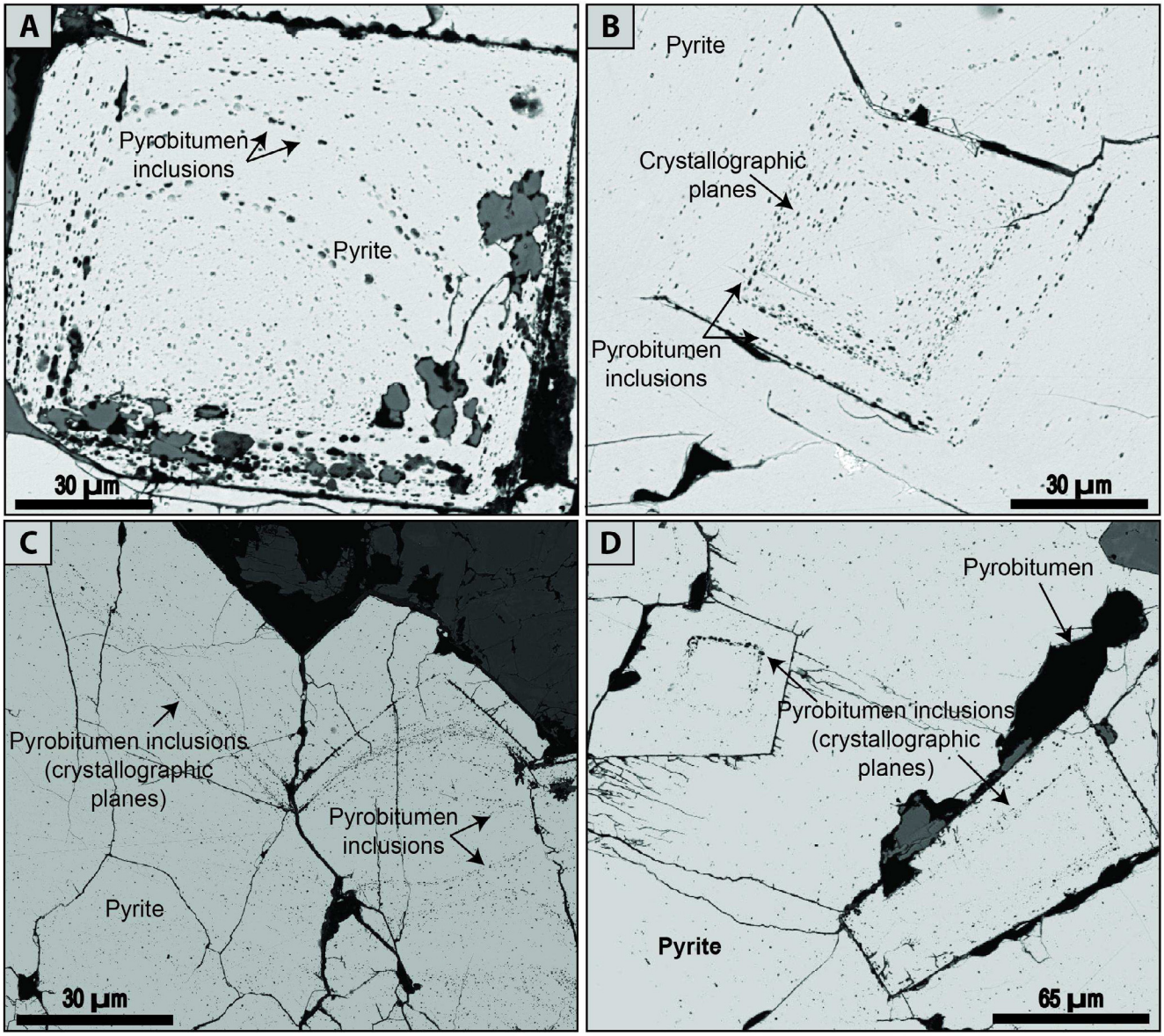

Fig. 8. A-D) Field emission scanning electron microscopy (FE-SEM) images revealing the presence of micro- to nano-sized pyrobitumen inclusions within Pyrite I. Pyrobitumen inclusions usually have droplet-like shapes and show a regular distribution following crystallographic planes. Pyrobitumen grains are also observed in fractures or near crystal rims.

assemblages are identified (Maureira, 2018). The hypogene stage comprises two sub-stages, i.e., a pre-ore and a main-ore stage. At Las Luces, the pre-ore stage is characterized by the presence of magnetite and pyrite, with minor chalcopyrite and hematite. In this event, pyrite is replaced by chalcopyrite in fractures. The main ore (Cu) stage is characterized by bornite-chalcocite assemblages with myrmekitic textures. The (late) supergene stage, on the other hand, is characterized by the formation of fine aggregates of digenite/covellite replacing hypogene chalcocite, and minor quantities of azurite and malachite are recognized (Maureira, 2018). Our paragenetic observations at the Lorena deposit (Fig. 16) are thus in agreement with those described for Las Luces. At Lorena, the pre-ore stage is characterized by the presence of pyrite grains that are intimately associated with globular pyrobitumen (OM1). This assemblage is common, for example, in the drill core segment 98.6 – 167 m (Fig. 4C, D). The main Cu ore stage, as described, consists of chalcocite, bornite and chalcopyrite, where chalcocite occurs as disseminated aggregates filling fractures, and is also intimately associated with angular pyrobitumen (OM3) (167 – 312 m, Fig. 4E, F). Pyrobitumen inclusions in pyrite and chalcocite (OM2) are present mostly in the deeper part of the drillcore (167–312 m, Fig. 4E, F; Figs. 8, 9, 10). Although the precise paragenetic position of the micro- to nano-sized pyrobitumen inclusions is difficult to constrain, they are interpreted here to have formed during both the pre-ore stage (i.e., pyrobitumen inclusions in pyrite) and the ore stage (i.e., pyrobitumen inclusions in chalcocite).

The paragenetic sequence (Fig. 16) and the occurrence of sulfide-pyrobitumen assemblages at Lorena is similar to those previously described for the pyrobitumen-bearing, Lower Cretaceous stratabound Cu deposits in central and northern Chile (e.g., El Soldado: (Zentilli et al., 1997; Wilson and Zentilli, 1999; Wilson et al., 2003a,b); Talcuna-Uchumi: (Wilson and Zentilli, 2006; Carrillo-Rosúa et al., 2014); and deposits near Copiapó: (Cisternas et al., 1999; Haggan et al., 2003; Cisternas and Hermosilla, 2006). In these deposits, the intimate association of pyrobitumen with Cu mineralization has been considered a key factor in the genesis of the stratabound orebodies, and two genetic stages have been recognized, i.e., a pre-ore stage involving thermal

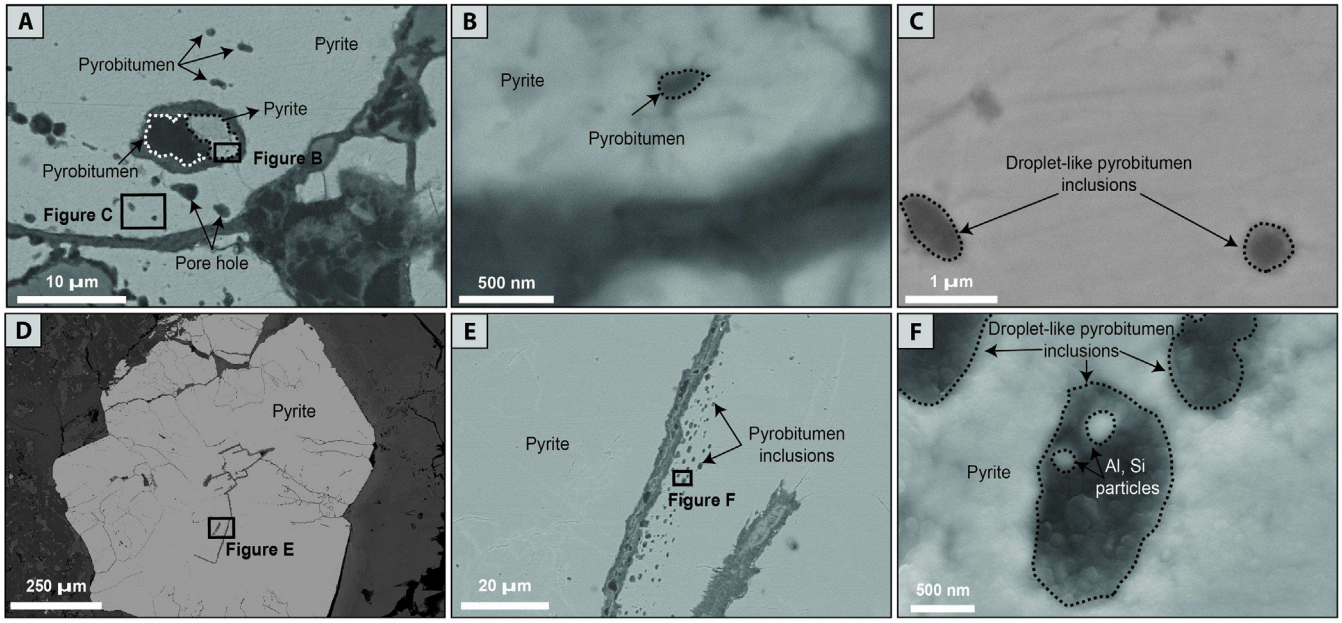

Fig. 9. Detailed FE-SEM images of micro- to nano-sized pyrobitumen inclusions in Pyrite I. A) Elongated, sub-rounded pyrobitumen inclusions within a pyrite grain. Pores are also observed. B) Detail view of nano-sized pyrobitumen droplet in pyrite inclusion observed in image (A). C) Rounded and elongated pyrobitumen nano-inclusions from image (A). D) Pyrobitumen inclusions bordering a fracture in the center of a pyrite grain. E) Detail view of pyrobitumen inclusions observed in D. F) Al- and Si-bearing nanoparticles within a pyrobitumen droplet.

degradation of oil-bearing brines resulting in the accumulation of pyrobitumen, followed by an ore stage where previously formed pyrite was replaced by Cu sulfides (Carrillo-Rosúa et al., 2014). The most accepted model for these deposits involves, therefore, the introduction of externally derived Cu-rich hydrothermal fluids. The hydrothermal fluids, independently of their proposed origin (e.g., magmatic-hydrothermal, basinal, meteorically-derived or mixed), interacted with the pyrobitumen-bearing pre-ore assemblages to form Cu sulfides, either by replacement or direct precipitation. Since the occurrence of pyrobitumen is distinctive and has not been previously reported in the Jurassic Las Luces district (or any other Jurassic stratabound Cu deposit in northern Chile), it is important to highlight that the Lorena deposit shares common attributes with the pyrobitumen-bearing deposits of the central Chile Lower Cretaceous belt (Fig. 1).

At Lorena, the pre-ore stage assemblage is characterized by the presence of pyrobitumen and pyrite and widespread albite alteration that affected the andesite host rock. Chlorite, zeolites, prehnite-pumpellyite, calcite and minor chalcedony, as well as pyrobitumen, are found filling vesicles and in the breccia matrix (Fig. 5). This assemblage has been recognized in other stratabound deposits that some authors have interpreted as formed by regional low-grade metamorphism prior to the hydrothermal event (Losert, 1973; Boric et al., 2002; Cisternas and Hermosilla, 2006; Carrillo-Rosúa et al., 2014).

Our observations suggest that the pre-ore assemblage formed when petroleum was mobilized from the source rock into the La Negra andesites by aqueous (connate?) fluids, precipitating pyrite as early phase. This resulted in the incorporation of pyrobitumen droplets into pyrite during sulfide growth from the solution. Therefore, pyrobitumen inclusions (OM2) within pyrite crystals point to coexistence between aqueous fluids and hydrocarbons during the first stage of formation of the deposit (pre-ore stage). This is in agreement with data reported by Wilson et al. (2003) for the El Soldado deposit in central Chile. Considering the coexistence of pyrobitumen, pyrite and low-grade alteration minerals in vesicles, it is likely that petroleum migration was probably synchronous with regional alteration related to low-grade (burial) metamorphism (Wilson and Zentilli, 1999; Wilson et al., 2003a,b; Cisternas and Hermosilla, 2006; Rieger et al., 2008; Carrillo-Rosúa et al., 2014).

As described, two textural types of pyrite were found associated with pyrobitumen in Lorena, i.e., euhedral-subhedral pyrite grains (Pyrite I; Fig. 6A, 7A) and rosette-shaped spherules of pyrite (Pyrite II) which suggest apparent growth from early pyrite cores (Fig. 6C, D). These two types are indicative of at least two events of pyrite formation. The rosette-like aggregates are interpreted as continuous growth from a pyrite core/seed into subhedral aggregates. On the other hand, the euhedral-subhedral pyrite type shows distinctive micro- to nano-sized pyrobitumen inclusions (OM2) (Fig. 9). The pyrobitumen inclusions (OM2) are arranged following a concentric pattern from the pyrite core, where pyrobitumen inclusions are randomly distributed, to the outer sections of the pyrite grain where inclusions are arranged following crystallographic planes (Fig. 8). The textural occurrence of pyrobitumen inclusions within pyrite crystals strongly suggests that pyrite grew in the presence of petroleum, as it happens in detrital grains (quartz and feldespar) along migration pathways or in reservoirs where petroleum inclusions are trapped (Munz, 2001).

The main ore (Cu) stage is characterized by minor chalcopyrite, bornite and chalcocite. Hypogene chalcocite was also precipitated directly, filling vesicles and fractures (Fig. 6G, H). In both cases, chalcocite can be observed accompanied by pyrobitumen (OM1 – OM3), however, textural observations show that chalcocite filling vesicles is mainly in contact with globular pyrobitumen (OM1) or replacing it, indicating that Cu sulfide precipitation was redox-induced by the presence of organic matter. On the other hand, chalcocite in fractures is associated with the more angular type of pyrobitumen (OM3) (e.g. Fig. 3C), most likely representing a later pulse of pyrobitumen or a (globular) pyrobitumen remobilization event (Fig. 3A). In addition, the presence of micro- to nano-sized pyrobitumen inclusions; within chalcocite grains (Fig. 6H; Fig. 10) indicate that (liquid) hydrocarbon phases were not restricted to the pre-ore stage, but were also present during the ore stage. During the main Cu event, pyrobitumen could have been in a semi-solid state induced by fluid mixing, water-washing and/or an increase in temperature (Wilson, 1998).

Covellite, digenite-djurleite and Cu oxide minerals (mainly chrysocolla and malachite) are only minor phases in Lorena and are indicative of a late supergene event. This mineral assemblage was formed by in-situ replacement/oxidation of primary (hypogene) Cu sulfides and

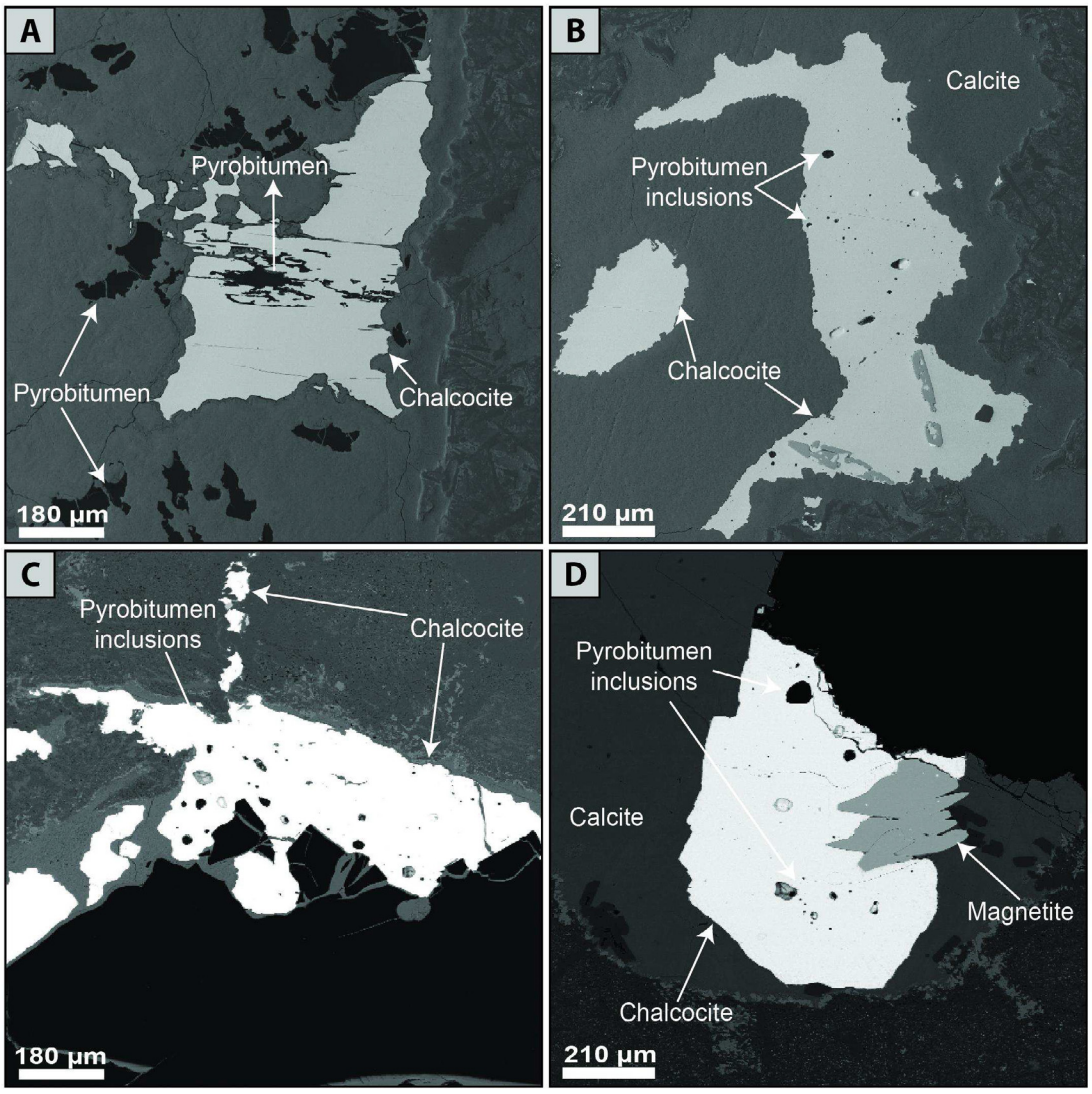

Fig. 10. Backscattered electron (BSE) images showing pyrobitumen in association with chalcocite. A) Angular pyrobitumen in close proximity to anhedral chalcocite grains. Also observed is pyrobitumen filling fractures in chalcocite. B) Rounded and randomly oriented inclusions of pyrobitumen within chalcocite. C) Angular pyrobitumen is observed in contact with and partially surrounded by chalcocite. Rounded pyrobitumen inclusions in chalcocite are also present. D) Chalcocite grain in contact with pyrobitumen and magnetite in a calcite amygdale. Pyrobitumen droplets within chalcocite are also observed.

occurs in vesicles and isolated masses (Fig. 3D). The lack of a relevant supergene, secondary sulfide blanket is possibly related to the minor presence of pyrite and hence, sulfuric acid production by sulfide weathering.

5.2. Evidence for hydrocarbon-hydrothermal fluid emulsions

The timing of pyrobitumen introduction in stratabound Cu-(Ag) deposits has been considered to pre-date the Cu mineralization event (Wilson and Zentilli, 1999; Cisternas and Hermosilla, 2006; Rieger et al., 2008; Carrillo-Rosúa et al., 2014). Observations at the Lorena deposit reveal the presence of pyrobitumen in both stages, i.e., in the pre-ore stage and the main Cu event. A first (initial) pulse is represented by globular pyrobitumen (OM1) and pyrite mainly, filling vesicles in the intermediate zone of the deposit (Fig. 4). Globular pyrobitumen (OM1) is partially replaced by Cu-(Fe) sulfides (chalcocite and bornite) (Fig. 6G). This indicates that the metal-bearing hydrothermal fluid could have interacted with pre-existing organic matter, which is capable of reducing complexed metals in solution to form sulfides (Dissanayake et al., 1993). In addition, a later pulse of hydrocarbons is represented by angular pyrobitumen (OM3) intergrown with Cu sulfides and calcite. This assemblage suggests that during the ore stage hydrocarbons were introduced either as a new, fresh pulse or re-mobilized from pre-existing (globular) pyrobitumen.

Most importantly, the presence of micro to nano-sized pyrobitumen inclusions within pyrite and chalcocite (Fig. 6H, 8, 10) points, unequivocally, to coexistence between hydrothermal fluids and hydrocarbons during the evolution of the deposit. Droplet-like pyrobitumen inclusions (OM2) within sulfides indicate the presence of liquid hydrocarbons during crystal growth as fine, immiscible oil droplets (petroleum) in a water emulsion. Water in the hydrothermal fluid could act as the dispersion medium (continuous phase) of micron-sized oil droplets (Sjöblom, 2001; Bibette et al., 2002). Individual droplets could have formed larger aggregates and/or rearranged at the water/oil interface (Langevin et al., 2004). Water-oil emulsions stability is dependent on several factors including viscosity, which is influenced by temperature and water content among other factors (Chen and Tao, 2005). The occurrence of small size (~500 nm) pyrobitumen inclusions within pyrite (Figs. 8 and 9) could be indicative of aqueous emulsion stability, where solution properties such as pH and temperature would have prevented the coalescence of smaller droplets into larger particles (e.g., 1–10 µm or larger). In addition, Si- and Al-bearing particles found

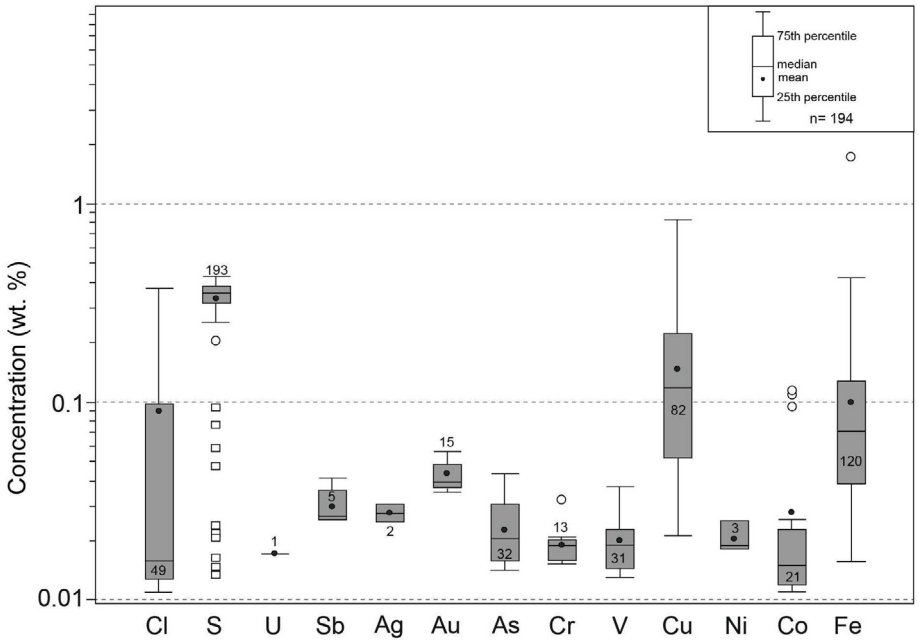

Fig. 11. Concentration boxplot for selected minor elements in pyrobitumen from Lorena. Electron microprobe analyses (EMPA) are plotted in weight percent (wt.%) on a vertical logarithmic scale. In the boxplot, mean and median concentrations are shown, as well as the number of analyses above detection limit for each element (displayed in or outside of each box). A circle outlier is a data point above 1.5 × (75th percentile - 25th percentile).

within the pyrobitumen inclusions (Fig. 9F) could have increased the stability of the emulsion, as documented for particles in crude oil or in seawater suspended sediments (Lee, 1999). Energy and mixing time are other important factors for emulsifications, where the latter makes the emulsifier more effective (Chen and Tao, 2005). Water-oil emulsions have been proposed to play a role in the formation of stratabound Cu deposits in central Chile. (Wilson and Zentilli, 1999) and (Wilson et al., 2003a) interpreted that pyrobitumen globules associated with framboidal pyrite at the El Soldado deposit may represent original droplets of semi-liquid petroleum. Droplets of oil were probably generated in the source rocks, coalesced and migrated with connate waters as an emulsion following a hydraulic gradient (Wilson, 1998). Spheres and globules of pyrobitumen identical to those observed at El Soldado and Lorena, have also been described in Mississippi Valley-type Pb-Zn deposits (Marikos et al., 1986; Gregg and Shelton, 2012) and Californian Hg deposits (Peabody et al., 1993). These studies have proposed that mineralization is associated with the generation and migration of hydrocarbons, which often mix with waters of various origins to form water-oil emulsions.

At Lorena, the formation and stabilization of a water-oil emulsion could have occurred as a result of convection and fluid mixing in the volcano-sedimentary sequences, triggered by temperature changes induced by either regional low-grade (burial) metamorphism, the intrusion of dikes, and/or thermal effects related to deep-seated intrusions (e.g., (Kojima et al., 2009). There are no fluid inclusion data from Lorena but microthermometric studies of Jurassic and Lower Cretaceous deposits have reported homogenization temperatures mostly within the 150 – 360 °C range (Maksaev et al., 2007; Kojima et al., 2009). Experimental studies have shown that heating to ~93 °C can result in an emulsified crude oil-water mixture (Cartmill and Dickey, 1970). Other experiments have shown that crude oil affected by temperatures close to 200 °C behave as low temperature liquid phases, although temperature degradation processes are likely to start at 250 °C (Migdisov et al., 2017). Potentially, the Lorena pyrobitumen was exposed to temperatures ranging from ~100 to 300 °C, coeval to pyrite crystallization during the pre-ore stage, which resulted in the incorporation of pyrobitumen droplets during sulfide growth from the aqueous fluid. Observations at Lorena also show pyrobitumen inclusions in chalcocite from the main Cu mineralization stage. These inclusions are scarcer than those in pyrite, and have a random

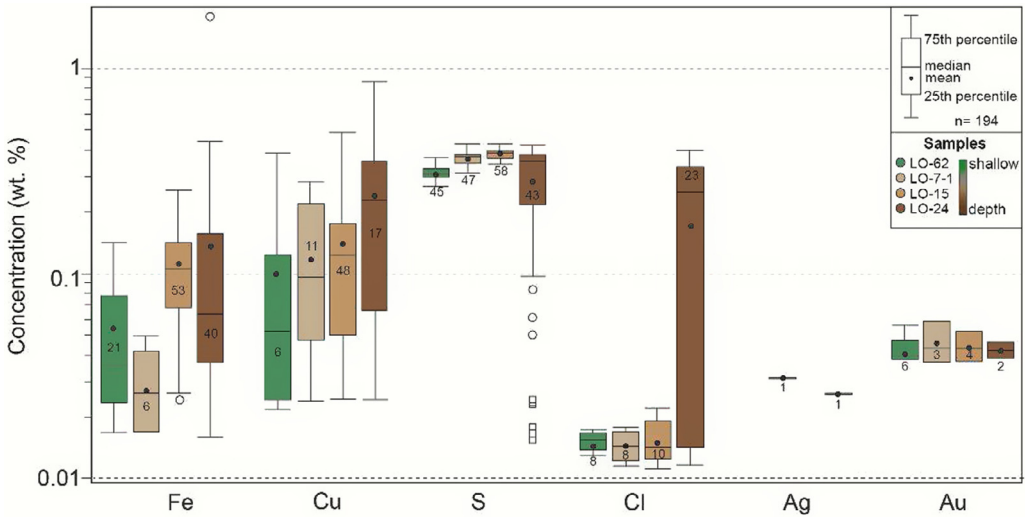

Fig. 12. Boxplot showing the concentration of Fe, Cu, S, Cl, Ag and Au in pyrobitumen plotted as a function of sample depth (LO-62, LO-7-1 and LO-15: intermediate-shallow samples, LO-24: deep sample). EMPA data are plotted in weight percent (wt%) on a vertical logarithmic scale. In each boxplot, mean concentrations are marked and the number of analyses above detection limit for each element is displayed inside/out of each box. A circle outlier is above 1.5 × (quartile 3-quartile 1) while a square outlier is above 3.0 × (75th percentile − 25th percentile).

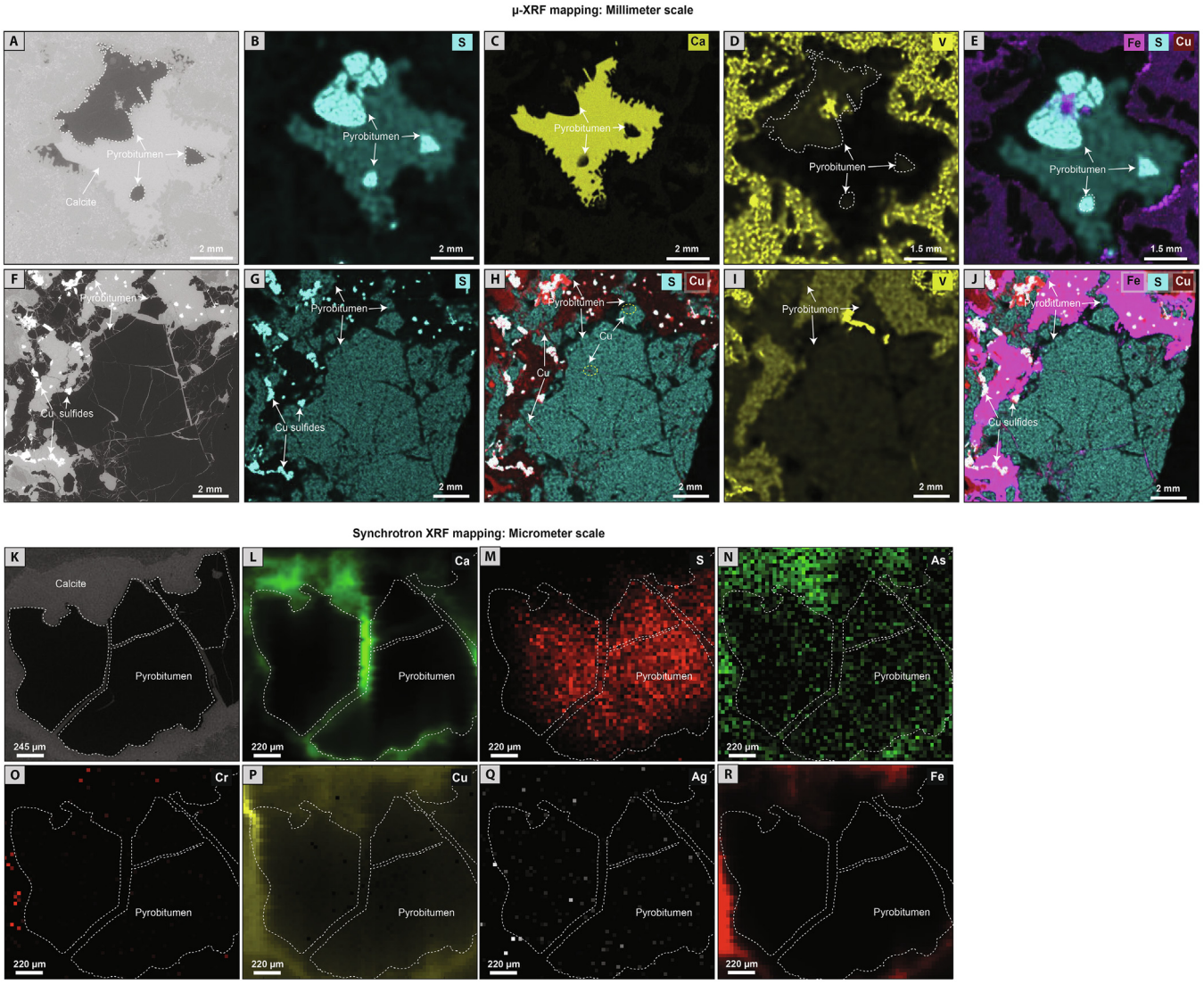

Fig. 13. XRF elemental maps of pyrobitumen grains from Lorena obtained by desktop (B-J) and synchrotron (L-R) μ-XRF. A, F, K) Backscattered electron (BSE) images of the analyzed pyrobitumen grains. See text for discussion.

distribution within the sulfide crystals and show rounded and sigmoid shapes (Fig. 6H, 10B-D). This suggests that pyrobitumen was probably in lower concentrations in a water-oil emulsion destabilized and/or in a semi-liquid state when hypogene chalcocite crystallized from hydrothermal Cu-rich fluids, precipitating at temperature > 150 ˚C (Mathur et al., 2018).

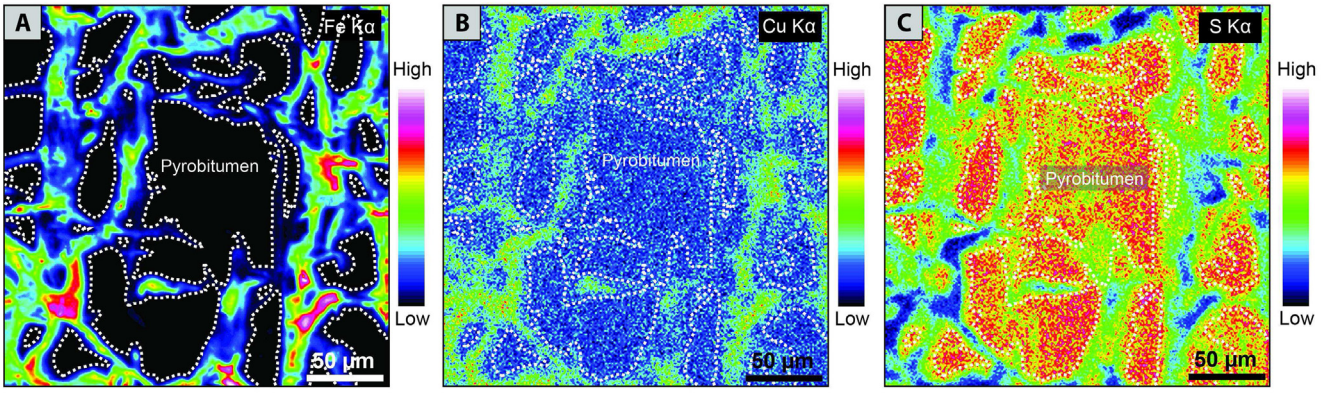

Fig. 14. Wavelength dispersive spectrometry (WDS) EMPA X-ray maps (Fe, Cu, S) of pyrobitumen grains within andesite host rock. The WDS maps show a high concentration of S and a low concentration of Cu in pyrobitumen. Slight variations in the S concentration are observed in the pyrobitumen grains, whereas Cu appears more homogeneous. No Fe was detected in the analyzed grains.

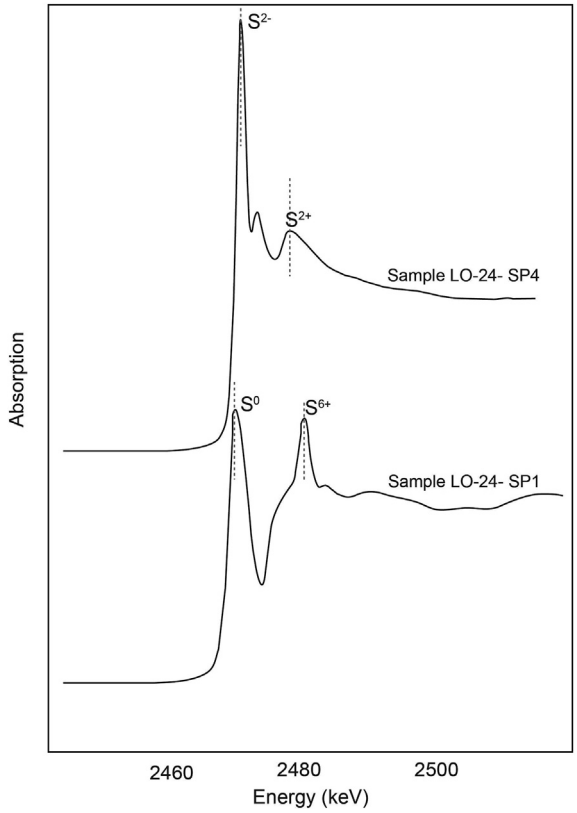

Fig. 15. Sulfur speciation in pyrobitumen obtained using synchrotron XANES. Several analyses were performed and merged to achieve each spectrum. XANES data of pyrobitumen from the Lorena deposit indicate the presence of thiophene and sulfone species (LO-24-SP4). Sample LO-24-SP1, on the other hand, shows peaks associated with elemental sulfur and sulfate.

5.3. Key metals in bitumen

Although limited data of trace and minor element on pyrobitumen are available, the role of hydrocarbons during metallogenesis has been explored in several mineralized systems (e.g., Manning et al., 1993; Wilson and Zentilli, 1999; Wilson and Zentilli, 2006; Fuchs et al., 2016). These studies have suggested that organic matter may have acted as a source or carrier of metals including Au (e.g., Carlin-type deposits in Nevada, Emsbo et al., 2007), U and Ti (e.g., Witwatersrand Au deposits, Fuchs et al., 2015), Pb (e.g., Laisvall Pb-Zn deposit, Saintilan et al., 2019), and V (e.g., Western Cordillera, Central Perú, Haggan and Parnell, 2000). Furthermore, Manning et al. (1993) suggested that petroleum liquids are potentially capable of transporting Cu. In fact, earlier investigations have reported high Cu concentrations in crude oil (0.01–28 ppm Cu; Colombo and Sironi, 1961; Colombo et al., 1964; Jones, 1975; Ali et al., 1983; Ellrich et al., 1985; Duyck et al., 2008), suggesting that Cu can substitute Ni and V in porphyrin-like structures in petroleum, which are abundant in natural oils (Manning et al., 1993). The chemical composition of pyrobitumen obtained in this study reveals significant concentrations of base metals at Lorena, e.g., high Cu and Fe concentrations (average of 0.16 and 0.1 wt %, respectively). Precious metals such as Au (and some Ag) were also detected. Ligands (Cl and S) also exhibit high concentrations, with average values of 0.09 and 0.34 wt% for Cl and S, respectively (Fig. 11).

Since Cu and other metals such as Fe are particularly high in pyrobitumen at Lorena, one further aspect to evaluate is whether these elements were originally enriched in the hydrocarbon phase or if the high concentrations are the result of the interaction of Cu-rich hydrothermal fluids with the pre-existing hydrocarbons. The main limitation to address this issue relates to the fact that published trace element data of pyrobitumen or liquid hydrocarbons is generally, very sparse. Also, as for the present study case at Lorena, available data corresponds to pyrobitumen in ore deposits and not the organic material from the source rocks or the original and unmodified migrated hydrocarbons. Available pyrobitumen EMPA data reported by Wilson and Zentilli (1999) for the El Soldado deposit are in agreement with microanalytical data presented here (Fig. 11). Microprobe analyses of isotropic cores of pyrobitumen grains show Cu ~ 0.7 wt%, Pb ~ 2.8 wt% and Cl of up to 2.25 wt%, while the anisotropic, hydrothermally disturbed domains contain more Cu (> 1 wt%), some Fe (~0.5 wt%), S (> 1 wt%), less Pb (0.7–1 wt%), and generally less Cl (< 1 wt%) (Wilson and Zentilli, 1999). This is interpreted by those authors as evidence that components of the hydrothermal fluid (Cu, S and Cl) were incorporated into pyrobitumen as a result of metasomatic processes during the Cu mineralization stage.

It is well documented that hydrocarbons and organic matter can contain significant amounts of metals, although evaluating the contribution of petroleum-derived metals to mineralization remains challenging. Recent experiments to determine the isothermal bulk solubility of selected metals in crude oil have demonstrated that metals such as Au, Zn and U can be efficiently transported and re-deposited by hydrocarbons. For example, at temperatures < 250 °C, solubility of Zn in crude oil is ~28 ppm (Migdisov et al., 2017), which is considered sufficient for the formation of a Mississippi Valley-type deposit (Leach et al., 2006). Pyrobitumen extracted from shale rocks, on the other hand, can have high concentrations of Zn (from 41 to 24,125 ppm) and Pb (between 3 and 400 ppm), suggesting that petroleum-derived Pb could make large contributions to ore formation (Saintilan et al., 2019). For the particular case of Cu, no experiments have been conducted to determine the solubility of this metal in liquid hydrocarbons and only traditional theoretical considerations have been proposed (Manning et al., 1993). Calculated stability indices of metal-organic compound (metalloporphyrins) for Cu^{2+} and other metals ions (e.g., VO^{2+}, Pd^{2+}, Ni^{2+}, Co^{2+}, Fe^{2+}, Zn^{2+}, Pb^{2+}) predict the empirical potential capacity of liquid petroleum to transport metals. These stability indices were determined based on ionic charge, electronegativity and ionic radius (Buchler and Smith, 1978; Manning et al., 1993) with VO^{2+}, Ni^{2+} and Zn^{2+} exhibiting values of 11.05, 6.8 and 4.1, respectively, indicating a high solubility for these cations. The calculated stability index for Cu^{2+} metal-organic compounds is 6.1, indicating that Cu could be potentially transported by liquid petroleum. However, this should be demonstrated experimentally and evaluated thoroughly in future studies.

At the Lorena deposit, mineralogical observations and WDS elemental maps show that the highest concentrations of Cu in pyrobitumen occur surrounding globular grains and within fractures (Fig. 14). Therefore, the evidence presented here strongly suggests that Cu detected in bitumen was most likely sourced from an external aqueous fluid that migrated through the pre-ore assemblage rather than from the hydrocarbon phase. We conclude that most of the Cu in Lorena was introduced to the system from external Cu-rich hydrothermal fluids during the main ore stage in agreement with previous studies (Wilson and Zentilli, 1999; Cisternas and Hermosilla, 2006; Carrillo-Rosúa et al., 2014). However, the possibility that pyrobitumen may have provided at least a small fraction of Cu and other components at Lorena cannot be ruled out. FE-SEM observations reveal angular Cu-Fe sulfide nanocrystals ~500 nm in size that are immersed within pyrobitumen grains (Fig. 17). Although the origin of these Cu-Fe nanocrystals cannot be fully assessed, recent studies have provided mineralogical and geochemical evidence that the presence of individual and complex nanocrystals could also reflect time-dependent growth of metals within a hydrocarbon phase (Fuchs et al., 2015).

5.4. Pyrobitumen as a source of organic sulfur

XANES data of pyrobitumen in the Lorena deposit show different species of sulfur including thiophene, elemental, sulfone and sulfate

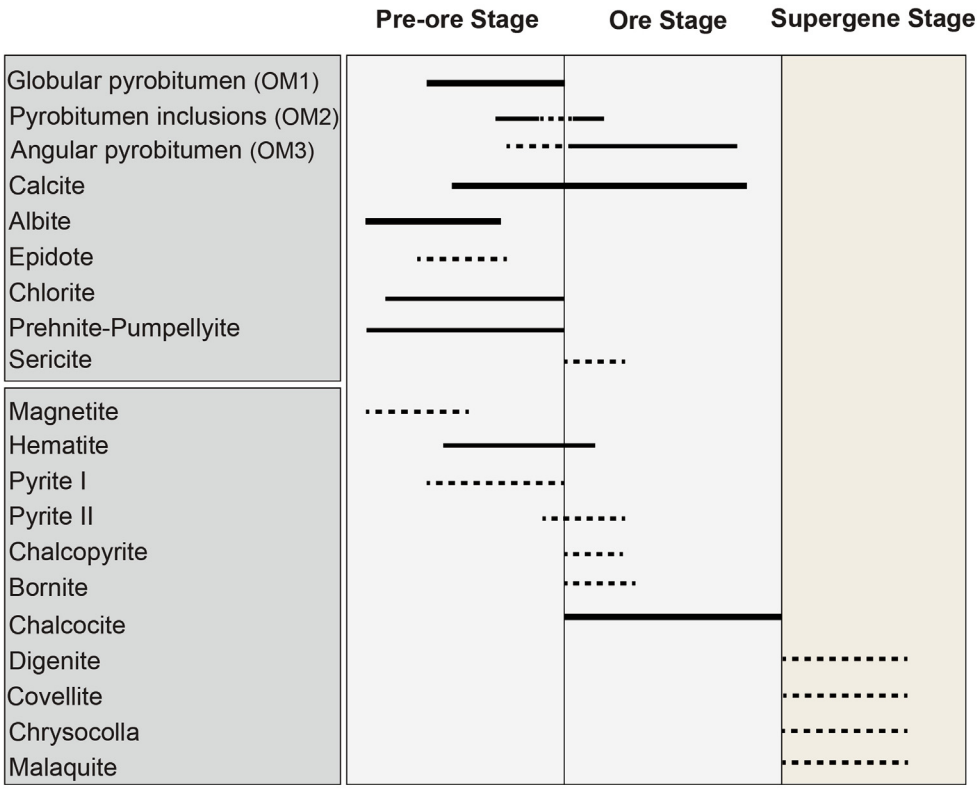

Fig. 16. Paragenetic sequence for the Las Luces deposit. The thick bars represent more abundant phases (dashed line, thin line and thick bar indicate low, moderate and abundant, respectively).

(Fig. 15). These sulfur species are dominant in kerogen, pyrobitumen, asphaltene and coals (Gorbaty et al., 1990; Kelemen et al., 2007; Lewan, 2007; Le Doan et al., 2013; Pomerantz et al., 2014; Bolin et al., 2016). Although the XANES data reported here are the first synchrotron measurements in bitumen in Chilean deposits, organic geochemistry data by (Rieger et al., 2008) for bitumen-bearing Lower Cretaceous deposits in the Copiapó area (~200 km south of Lorena) allow for some comparisons. Analyses of the molecular composition of aliphatic and aromatic compounds performed in pyrobitumen samples by Rieger et al. (2008) showed that total aromatic hydrocarbon fraction in this location exhibits an unusually high percentage of sulfur-bearing components (thioaromatics) with dibenzothiophenes, naphthobenzothiophenes and dinaphthobenzothiophenes; the latter being most abundant. These results indicate that a potentially significant fraction of sulfur in the pyrobitumen has thioaromatic components such as thiophene, i.e., sulfur in an aromatic ring. This is one of the most common forms of sulfur reported in pyrobitumen (Birdwell et al., 2018) and the most thermally stable form of organic sulfur in petroleum (Huffman et al., 1991). Hence, thiophene is expected to occur as a large fraction of the total sulfur present in pyrobitumen associated with petroleum source rocks (Bolin et al., 2016). Elemental sulfur, on the other hand, typically occurs in natural crude oil (Eccleston et al., 1952; Pomerantz et al., 2014; Greenfield et al., 2015), while sulfone can be derived from the oxidation of organic sulfur compounds under elevated temperature (Gorbaty et al., 1992), including the oxidation of pyrobitumen. Oxidation of organic matter during the formation of sulfide ores has been documented in sedimentary hosted Pb-Zn deposits (Pratt et al., 1998) and at the El Soldado Cu deposit. (Wilson and Zentilli, 1999) proposed that CO_2 resulting from bitumen oxidation formed calcite. Our exploratory XANES data of sulfur speciation in pyrobitumen suggest that thiophene and elemental compounds are dominant sulfur species at Lorena, and results are indicative of the presence of organosulfur compounds that can be attributed to an organic source for this element in pyrobitumen. The formation of sulfone and sulfate species, on the

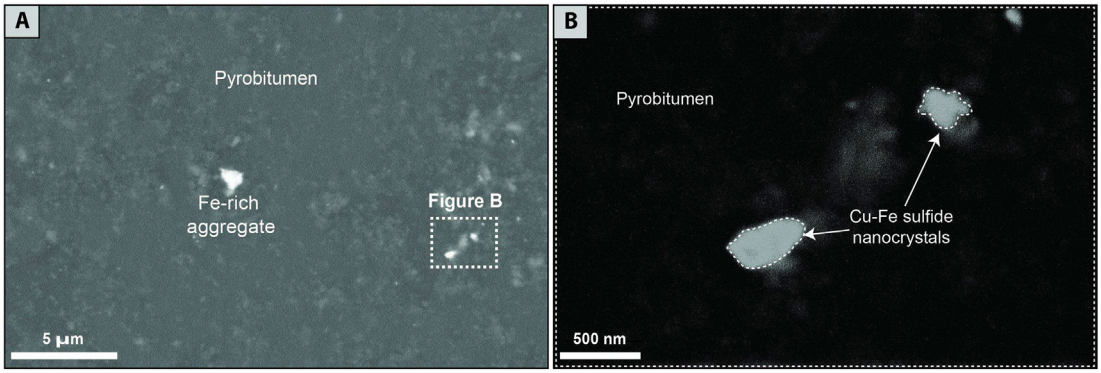

Fig. 17. FE-SEM BSE images showing micro- to nano-sized Cu-Fe sulfide inclusions within pyrobitumen. The BSE image on the right (B) shows a magnified view of the ~250 to 500 nm Cu-Fe sulfide nanocrystals.

other hand, may have resulted from modification (probably oxidation) of the organic compounds at higher temperature, during the main ore stage, when externally derived Cu-rich hydrothermal fluids circulated through pyrobitumen, as suggested by (Wilson and Zentilli, 1999) for the El Soldado deposit.

Although the organic origin of sulfur in the pyrobitumen at Lorena is unknown, a possible source could be the same sedimentary rocks that probably generated the hydrocarbons, e.g., the Pan de Azúcar or the Las Tórtolas formations (Fig. 2). Even though Lower Jurassic rocks are not a particularly fertile hydrocarbon source worldwide, the Hettangian-Sinemurian shows evidence of inhospitable, sulphurous seas along many coasts (e.g., Richoz et al., 2012). In the ancestral Chilean Coast the late Triassic was a low-stand with deep erosion, but the early Jurassic deposited fossil-rich beds when sealevel rose during transgression. If petroleum was an important element helping to concentrate pyrite (and hence sulfur) during liquid oil maturation, migration and concentration, it probably had the same potential in many areas where the Pan de Azúcar Fm. is preserved under the volcanics. This should be taken into account in future studies assessing prospectivity surveys in the district.

In sedimentary rocks, the largest fraction of the organic sulfur is in the high-molecular-weight form, which can be inherited in the residual products like pyrobitumen formed after diagenesis and generation processes of hydrocarbons. Sulfur concentrations in organic-rich sedimentary rocks, such as black shales, can be higher than 6 wt% (Wedepohl, 1978). Diagenetic processes of these rocks can form different types of light, moderate and heavy hydrocarbons, and asphaltenes. These organic phases can incorporate a large amount of the sulfur available in the source rock and are rich in asphaltenes (i.e., high molecular weight compounds with significant N, S and O heteroatoms) (Parnell, 1993), which when accompanied by heavy aromatics, can accommodate most of the sulfur compounds in hydrocarbons (Speight, 1991), with concentrations ranging from 0.07 to 10 wt% (Rospondek et al., 1994; Riazi et al., 1999).

Pyrobitumen (OM1 and OM3) from the Lorena deposit hosts significant concentrations of sulfur (Figs. 11 and 12). Small variations were found along the drill core with slightly higher sulfur concentrations in the intermediate section with respect to the lower section (average of 0.35 to 0.28 wt%, respectively). These variations most likely reflect the depletion and/or enrichment of sulfur in pyrobitumen as a result of interaction with hydrothermal fluids. X-ray elemental maps of sulfur in this pyrobitumen show that sulfur is homogenously distributed within grains (Fig. 13B, G), and probably reflect the primary sulfur content. In contrast, elemental sulfur maps in pyrobitumen from deeper levels (~289 m) display lower concentrations towards the grain rims (Fig. 13M), suggesting that sulfur decrease was probably caused by the chemical interaction with hydrothermal fluids. During this interaction, pyrobitumen was likely exposed to higher temperatures (> 100 to ~300 °C) under which geochemical changes, such as isomerization to lower steric energy and aromatization, can occur. Consequently, carbon bonds are broken, increasing electron unpairing (Gize, 1999) and sulfur release from the organic phase into the hydrothermal fluid.

Experimental evidence suggested that the solubility peak of some cations in pyrobitumen is achieved at temperatures above the oil window (Migdisov et al., 2017), where the upper limit is typically between 120 and 170 °C (Philippi, 1965). It is also known that the solidification of liquid petroleum and subsequent thermal cracking is associated with bond breakage (Landais and Gize., and Barnes, 1997), and at temperatures above 150 °C dehydrogenization reactions can be induced with emission of hydrogen sulfide (De Filippis et al., 1998; Masegosa et al., 2012). At Lorena, lower sulfur concentrations are observed in pyrobitumen grain rims (Fig. 13M), indicating that these grains where likely in contact with a high temperature hydrothermal fluid. This interaction would have caused chemical bond breakage and trigger the loss of external heteroatoms including thiols compounds from pyrobitumen and hence, sulfur from heteroatoms could have been incorporated into the hydrothermal fluid. Hydrogen sulfide (H_2S) loss from such reactions could have contributed, at least partially, to the sulfur budget available for sulfide mineralization during the ore stage, when hydrothermal fluids mixed with pyrobitumen. The interaction of pyrobitumen with Cu-bearing aqueous solutions would have triggered Cu sulfide precipitation assuming that Cu was transported as $CuCl_2^-$ (Akinfiev and Zotov, 2001; Akinfiev and Zotov, 2010). The pyrobitumen phase would in turn be oxidized during the interaction to form CO_2, which can also be incorporated in the fluid. This could explain the common association of chalcocite with pyrobitumen and calcite. Textural evidence for this hydrocarbon-triggered precipitation of Cu from hydrothermal fluids is provided by the occurrence of microscopic, angular particles that precipitate around and between pyrobitumen fractures (Fig. 5D, 10C-D). The bitumen-fluid interaction resulted in loss and addition of components from pyrobitumen as revealed by μ-XRF and EMPA data (Figs. 12 and 13), where high concentrations of chlorine and the lowest concentrations of sulfur were determined in angular pyrobitumen (OM3) from the deep zone. The evidence presented here suggests that at least a part of the sulfur in pyrobitumen could have been released slowly and gradually over time as pyrobitumen aromatizes. This aromatization would allow the loss of the outer rings, i.e., the thioaromatic components, releasing sulfur (i.e., H_2S) which is then incorporated in the hydrothermal fluids during the Cu ore stage.

6. Genetic model and concluding remarks

Mineralogical observations and geochemical data show evidence that Cu-(Fe) sulfides and pyrobitumen are intimately associated in the Lorena stratabound Cu-(Ag) deposit. Based on textural observations, two main events of hypogene mineralization were identified at Lorena: a pre-ore stage, characterized by the presence of pyrobitumen, pyrite and widespread albite alteration followed by an ore stage with abundant chalcocite, pyrobitumen, and minor chalcopyrite and bornite.

The study of pyrobitumen at Lorena is essential in understanding the processes involved in the formation of the deposit from the evolution of the organic phase to the pre-ore and ore stages (Fig. 18). The early stages involved hydrocarbon (petroleum) generation in the sedimentary source rocks (Fig. 18A, B), which was mobilized as immiscible droplets by aqueous (connate?) waters. Some micro- to nano-sized pyrite crystals were most likely formed and transported within the organic phase during this early pre-ore stage. Later, the migrated hydrocarbons were injected into the volcanic host rocks, filling vesicles and fractures (globular pyrobitumen, OM1) (Fig. 18C, D). At Lorena, the formation and stabilization of the water-oil emulsion could have occurred as a result of convection and fluid mixing in the volcano-sedimentary sequence, temperature changes induced by regional low-grade (burial) metamorphism, the intrusion of dikes, and/or thermal effects related to deep-seated intrusions. Pyrite II was formed around early pyrite cores (Pyrite I) in the presence of hydrocarbons, resulting in the incorporation of micro- to nano-sized pyrobitumen inclusions (OM2, Fig. 18D). During the ore stage, an externally derived Cu-rich hydrothermal fluid was introduced into the system and interacted with organic matter (pyrobitumen). The pyrobitumen/fluid interaction triggered Cu sulfide precipitation by redox processes (Fig. 18E, F). Evidence of a second event of hydrocarbon introduction or remobilization of the pre-existing pyrobitumen, OM1, during the Cu ore stage, is represented by the angular pyrobitumen (OM3). This close association between chalcocite and organic matter is also evidenced by the presence of pyrobitumen inclusions in chalcocite (OM2) (Fig. 18F). At the same time, metasomatic processes may have resulted in thermal cracking of the organic phase, resulting in chemical bond breakage and loss of sulfur, which was incorporated into the hydrothermal fluid.

Results presented here are in agreement with previous studies on Cretaceous stratabound Cu-(Ag) deposits in central Chile supporting the notion that pyrobitumen played a key role during ore formation as a redox trap for Cu sulfide precipitation. In addition, our data indicate

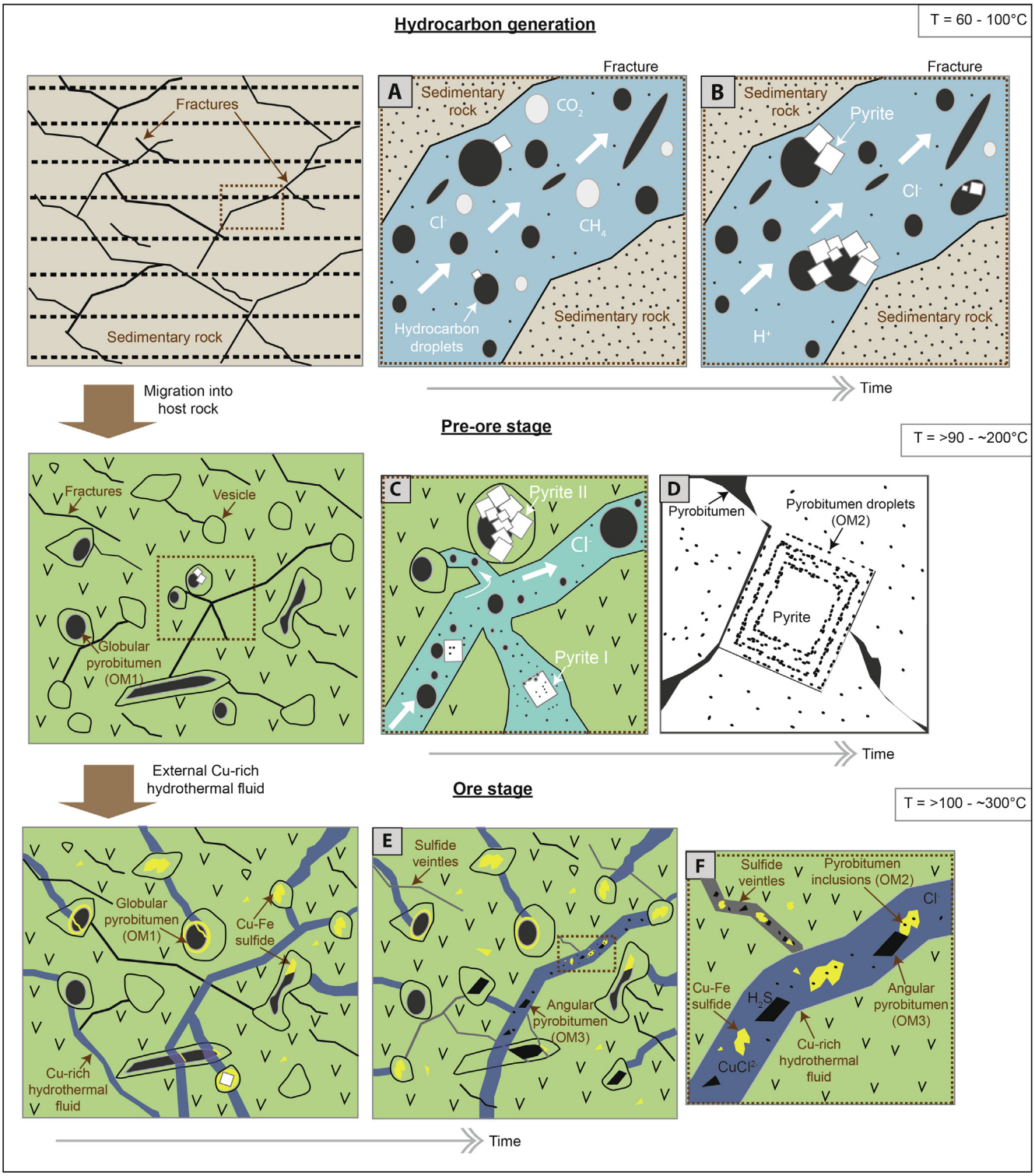

Fig. 18. Summary figure showing key processes that led to the formation of the bitumen-bearing Lorena stratabound Cu-(Ag) deposit. A) and B) The first stage involves hydrocarbon generation from a sedimentary rock source. Petroleum was mobilized as immiscible droplets in an aqueous fluid through permeability zones. At the same time, hydrocarbon gases are emitted (e.g., CH_4 and CO_2) and pyrite grains are bound by coalescence into the petroleum phase. C) and D) Migrated hydrocarbons were injected into the andesite rocks filling vesicles (OM1) and pyrite crystals grew in the presence of hydrocarbons (e.g., OM2). E) and F) External Cu-rich fluids circulated through the andesite host rock. The pyrobitumen-fluid interaction triggered Cu sulfide precipitation and a second pulse of hydrocarbon or remobilization event is evidenced by the presence of angular pyrobitumen (OM3) in close association with chalcocite (which can also show bitumen inclusions, OM2). At the same time, the organic phase is affected by thermal cracking, resulting in chemical bond breakage and leading to a slow, gradual released of sulfur as pyrobitumen becomes more aromatized. See text for details.

that at least some of the sulfur – and eventually some metals, such as Cu and Au – may have been sourced from pyrobitumen.

This is the first report of the occurrence of pyrobitumen in the Jurassic stratabound Cu-(Ag) deposits of northern Chile. It is uncertain at this point if this constitutes a unique case due to the presence of sedimentary rocks in the Las Luces district. Further studies are required not only to investigate the presence of bitumen in other Jurassic deposits but also to constrain the role of bitumen in ore formation in Chilean stratabound Cu-(Ag) deposits.

Declaration of Competing Interest

The authors declare that they have no known competing financial interests or personal relationships that could have appeared to influence the work reported in this paper.

Acknowledgments

Funding for this study was provided by Millennium Science Initiative (MSI) through “Millennium Nucleus for Metal Tracing Along Subduction” grant, and by FONDECYT project #1140780. The authors acknowledge support from FONDAP project #15090013 “Centro de Excelencia en Geotermia de los Andes, CEGA”. Research supported by the LNLS – Brazilian Synchrotron Light Laboratory, CNPEM/MCTIC is acknowledged, as well as travel funding by CNPEM. We thank technical assistance of Carlos Pérez, Dalton Abdala and Santiago Tassara during synchrotron analyses. We also thank technical assistance by Owen Neil during EMPA analyses at Washington State University. The FE-SEM instrument used in this study was funded by FONDEQUIP project EQM150101. We thank Compañia Minera Las Cenizas for providing access to drill core samples. Andrea Paola Herazo thanks financial support provided by a Doctoral scholarship from ANID (21171385) and the Hugh McKinstry grant from the Society of Economic Geologists Foundation (SEGF). We thank associate editor Si-Yu Hu for handling the manuscript. Yafei Wu and two anonymous reviewers are acknowledged for their helpful comments and suggestions.

Appendix A. Supplementary data

Supplementary data to this article can be found online at https://doi.org/10.1016/j.oregeorev.2020.103639.

References

Akinfiev, N.N., Zotov, A.V., 2001. Thermodynamic description of chloride, hydrosulphide, and hydroxide complexes of Ag(I), Cu(I), and Au(I) at temperatures of 25–500°C and pressures of 1–2000 bar. Geochem. Int. 39, 990–1006.

Akinfiev, N.N., Zotov, A.V., 2010. Thermodynamic description of aqueous species in the system Cu- Ag-Au-S-O-H at temperatures of 0–600°C and pressures of 1–3000 bar. Geochem. Int. 48, 714–720.

Ali, M.F., Bukhari, A., Saleem, M., 1983. Trace metals in crude oils from Saudi Arabia. Ind. Eng. Chem. Prod. Res. Dev. 22, 691–694.

Anderson, G.M., 1991. Organic maturation and ore precipitation in Southeast Missouri. Econ. Geol. 86, 909–926.

Barra, F., Reich, M., Selby, D., Rojas, P., Simon, A., Salazar, E., Palma, G., 2017. Unraveling the origin of the Andean IOCG clan: a Re-Os isotope approach. Ore Geol. Rev. 81, 62–78.

Bibette, J., Leal-Calderon, F., Schmitt, V., Poulin, P., 2002. Introduction, in: Emulsion science - Basic principles, Springer.

Birdwell, J.E., Lewan, M.D., Bake, K.D., Bolin, T.B., Craddock, P.R., Forsythe, J.C., Pomerantz, A.E., 2018. Evolution of sulfur speciation in bitumen through hydrous pyrolysis induced thermal maturation of Jordanian Ghareb Formation oil shale. Fuel 219, 214–222.

Bolin, T., Birdwell, M., Lewan, D., Hill, R., Grayson, M., Mitra-Kirtley, S., Bake, K., Craddock, P., Abdallah, W., Pomerantz, A., 2016. Sulfur species in source before and after hydrous pyrolysis determined by X-ray absorption near-edge structure. Energy Fuel. 30 (8), 6264–6270.

Boric, R., Díaz, F., Maksaev, V., 1990. Geología y Yacimientos Metalíferos de la Región de Antofagasta. SERNAGEOMIN, Santiago, Chile, Boletín 40, 246 (in Spanish).

Boric, R., Holmgren, C., Wilson, N.S.F., Zentilli, M., 2002. The geology of the El Soldado Manto Type Cu (Ag) Deposit, Central Chile. In: Porter, T.M. (Ed.), HydrothermAl Iron Oxide Copper-Gold & RelAted Deposits: A GlobAl Perspective, Volume 2. PGC Publishing, Adelaide, pp. 163–184.

Buchler, J.W., 1978. Synthesis and properties of metalloporphyrins. In: Smith, K.M. (Ed.), Porphyrins and MetalloPorphyrins. Elsevier, pp. 157–231.

Carrillo-Rosúa, J., Boyce, A., Morales-Ruano, S., Morata, D., Roberts, S., Munizaga, F., Moreno-Rodríguez, V., 2014. Extremely negative and inhomogeneous sulfur isotope signatures in Cretaceous Chilean manto-type Cu-(Ag) deposits, Coastal Range of central Chile. Ore Geol. Rev. 56, 3–24.

Cartmill, J.C., Dickey, P.A., 1970. Flow of a disperse emulsion of crude oil in water through porous media. Am. Assoc. Pet. Geol. Bull. 54, 2438–2447.

Chen, C., Tao, D., 2005. An experimental study of stability of oil-water emulsion. Fuel Process. Technol. 55, 143–151.

Cisternas, M.E., Frutos, J., Galindo, E., Spiro, B., 1999. Lavas con pyrobitumen en el Cretácico Inferior de Copiapó: petroquímica importancia metalogénica. Revista Geologica de Chile 26, 205–226 (in Spanish).

Cisternas, E., Hermosilla, J., 2006. The role of bitumen in strata-bound copper deposit formation in the Copiapó area, Northern Chile. Miner. Depos. 41, 339–355.

Colombo, U., Sironi, G., 1961. Geochemical analysis of Italian oils and asphalts. Geochim. Cosmochim. Acta 25, 24–51.

Colombo, U., Sironi, G., Fasolo, G.B., Malvano, R., 1964. Systematic neutron activation technique for the determination of trace metals in petroleum. Anal. Chem. 36, 802–807.

Crede, L.S., Liu, W., Evans, K., Rempel, K., Testemale, D., Brugger, J., 2019. Crude oils as ore fluids: an experimental in-situ XAS study of gold partitioning between brine and organic fluid from 25 to 250°C. Geochim. Cosmochim. Acta 244, 352–365.

Cucurella, J., Canut de Bon, C., Cisternas, M.E., 2005. Pyrobitumen related to silver-copper deposits in a Cretaceous volcanic-sedimentary sequence: Talcuna district, Coquimbo, Chile. Mineral. Polonica 36 (1), 21–29.

Cuney, M., 2009. The extreme diversity of uranium deposits. Miner. Depos. 44, 3–9.

Detlef, K., 2002. Geologisch-tektonische Karte der Küstenkordillere südlich von Taltas (Nordchile). Maβstab 1 (150), 000.

De Filippis, P., Giavarini, C., Santarelli, M.L., 1998. Sulphur-extended Asphalt: reaction Kinetics of H2S evolution. Fuel 77 (5), 463.

Dissanayake, C.B., 1993. Gold and other metals in graphite; in: Parnell, J., Kucha, H., Landais, P., (Eds.), Bitumen in ore deposits. Society for Geology Applied to Mineral Deposits, Sp 9, 138–152.

Duyck, C., Miekeley, N., Fonseca, T.C.O., Szatmari, P., dos Santos, Vaz, Neto, E., 2008. Trace element distributions in biodegraded crude oils and fractions from the Potiguar Basin. Brazil. J. Braz. Chem. Soc. 19 (5), 978–986.

Eccleston, B.H., Morrison, M., Smith, H.M., 1952. Elemental Sulfur in Crude Oil. Petroleum Experiment Station, Bureau of Mines, Bartlesville, Okla.

Ellrich, J., Hirner, A., Stark, H., 1985. Distribution of trace elements in crude oils from southern Germany. Chem. Geol. 48, 313–323.

Emsbo, P., Koenig, A.E., 2007. Transport of Au in petroleum: evidence from the northern Carlin trend, Nevada; in: Andrew, C.J., Borg, G. (Eds.), Digging Deeper, Proceedings of the Ninth Biennial SGA Meeting. Irish Association for Economic Geology, Dublin, pp. 695–698.

Espinoza, S., Véliz, H., Esquivel, J., Arias, J., Moraga, A., 1996. The cupriferous province of the Coastal Range, northern Chile; in: Camus, F., Sillitoe, R.H., Petersen, R. (Eds.), Andean Copper Deposits: New Discoveries, Mineralization, Styles and Metallogeny. Society of Economic Geologist Sp Pub 5, pp. 19–32.

Evans, K.A., Dyar, M.D., Reddy, S.M., Lanzirotti, A., Adams, D.T., Tailby, N., 2014. Variation in XANES in biotite as a function of orientation, crystal composition, and metamorphic history. Am. Miner. 99, 443–457.

Fuchs, S., Schumann, D., Williams-Jones, A.E., Vali, H., 2015. The growth and concentration of uranium and titanium minerals in hydrocarbons of the Carbon Leader Reef, Witwatersrand Supergroup, South Africa. Chem. Geo. 393–394, 55–66.

Fuchs, S., Williams-Jones, A.E., Przybylowicz, W.J., 2016. The origin of the gold and uranium ores of the Black Reef Formation, Transvaal Supergroup. South Africa. Ore Geol. Rev. 72, 149–164.

Gaupp, R., Moller, P., Lüders, V., di Primio, R., Littke, R., 2008. Fluids in sedimentary basin: an overview. Dynamics of Complex Sedimentary Basins – The Example of the Central European Basin System. 347-365.

García, F., 1967. Geología del Norte Grande de Chile, Simposio, Geosinclinal Andino, Sociedad Geológica de Chile. Publicaciones 3, 138 (in Spanish).

Gize, A.P., 1999. Organic alteration in hydrothermal sulfide ore deposits. Econ. Geol. 94, 967–980.

Gorbaty, M.L., George, G.N., Kelemen, S.R., 1990. Chemistry of organically bound sulphur forms during the mild oxidation. Fuel 69, 945–949.

Gorbaty, M.L., Kelemen, S.R., George, G.N., Kwiatek, P.J., 1992. Characterization and thermal reactivity of oxidized organic sulfur forms in coals. Fuel 71, 1255–1264.

Greenfield, M.L., Byrne, M., Mitra-Kirtley, S., Kercher, E.M., Bolin, T.B., Wu, T., Craddock, P.R., Bake, K.D., Pomerantz, A.E., 2015. XANES measurements of sulfur chemistry during asphalt oxidation. Fuel 162, 179–185.

Gregg, Jay M., and Kevin L. Shelton., 2012. Mississippi Valley-type mineralization and ore deposits in the Cambrian-Ordovician great American carbonate bank; in: J. R. Derby, R. D. Fritz, S. A. Longacre, W. A. Morgan, and C. A. Sternbach (Eds), The great American carbonate bank: The geology and economic resources of the Cambrian–Ordovician Sauk megasequence of Laurentia: AAPG Memoir 98, pp. 161–185.

Haggan, T., Parnell, J., 2000. Hydrocarbon-metal associations in the Western Cordillera, Central Peru. J. Geochem. Explor. 69–70, 229–234.

Hitchon, B., Filby, R.H., Shah, K.R., 1975. Geochemistry of trace elements in crude oils, Alberta, Canada; in Yen, T.F (Ed.), The Role of Trace Metals in Petroleum, Ann Arbor Science Publisher 111-112.

Haggan, T., Parnell, J., Cisterna, M.E., 2003. Fluid history of andesite-hosted CuS-bitumen mineralization, Copiapó district, north central Chile. J. Geochem. Explor.

78–79, 631–633.
Huffman, G.P., Mitra-Kirtley, S., Huggins, F.E., Shah, N., Vaidya, S., Lu, F., 1991. Quantitative analysis of all major forms of sulfur in coal by X-ray absorption fine structure spectroscopy. Energy Fuel. 5, 574–581.
Jones, P., 1975. Trace Elements and Other Elements in Crude Oil- A Literature Review. Report of British Petroleum Research Centre, Sunburry.
Kelemen, S.R., Afeworki, M., Gorbaty, M.L., Sansone, M., Kwiatek, P.J., Walters, C.C., Freund, H., Siskin, M., Bence, A.E., Curry, D.J., Solum, M.S., Pugmire, R.J., Vandenbroucke, M., Leblond, M., Behar, F., 2007. Direct characterization of kerogen by X-ray and solid-state ^{13}C nuclear magnetic resonance methods. Energy Fuel. 21, 1548–1561.
Khuhawar, M.Y., Mirza, M.A., Jahangir, T.M., 2012. Determination of Metal Ions in Crude Oils; in: Abdul-Raouf, M.E.-S. (Ed.), Crude Oil Emulsions – Composition Stability and Characterization. InTech, Croatia, 1-25, doi: 10.5772/36945.
Kojima, S., Tristá-Aguilera, D., Hayashi, K., 2009. Genetic aspects of the manto-type copper deposits based on geochemical studies of North Chilean deposits. Resour. Geol. 59 (1), 87–98.
Konecke, B., Fiege, A., Simon, A., Parat, F., Stechern, A., 2017. Co-variability of S6+, S4+, and S2- in apatite as a function of oxidation state: implications for a new oxybarometer. Am. Miner. 102 (3), 548–557.
Landais and Gize.,, 1997. Organic matter in hydrothermal ore deposits. In: Barnes, H.E. (Ed.), Geochemistry of Hydrothermal Ore Deposits, John Wiley & Sons. New York.
Langevin, D., Poteau, S., Hénaut, I., Argillier, J.F., 2004. Crude oil emulsion properties and their application to heavy oil transportation. Oil Gas Sci. Technol. Rev. IFP 59 (5), 511–521.
Large, R.R., Bull, S.W., Maslennikov, V.V., 2011. A carbonaceous sedimentary source-rock model for carlin-type and orogenic gold deposits. Econ. Geol. 106, 331–358.
Leach, D., Macquar, J.C., Lagneau, V., Leventhal, J., Emsbo, P., Premo, W., 2006. Precipitation of lead–zinc ores in the Mississippi Valley-type deposit at Trèves, Cévennes region of southern France. Geofluids 6, 24–44.
Le Doan, T.V., Bostrom, N.W., Burnham, A.K., Kleinberg, R.L., Pomerantz, A.E., Allix, P., 2013. Green River oil shale pyrolysis: semi-open conditions. Energy Fuel. 27, 6447–6459.
Lee, R.F., 1999. Agents which promote and stabilize water-in- oil emulsions. Spill Sci. Technol. Bull. 5, 117–126.
Lewan, M., 1984. Factors controlling the proportionality of vanadium to nickel in crude oils. Geochim. Cosmochim. Acta 48, 2231–2238.
Lewan, M.D., Hill, R.J.; in: Boak, J. (Ed.), Proceedings of the 27th Oil Shale Symposium, Colorado School of Mines: Golden, CO, 2007.
Losert, J., 1973. Genesis of copper mineralizations and associated alterations in the Jurassic volcanic rocks of the Buena Esperanza mining area, Departamento de Geología, Universidad. de Chile, 40, 64.
Lo Mónaco, S., López, L., Rojas, H., Lugo, P., García, D., Gastiel, J., 2007. Applications of electron microprobe analysis (EPMA) in the study of Venezuelan source rocks: La Luna and Querecual Formations. Fuel 86, 641–648.
Maksaev, V., Zentilli, M., 2002. Chilean strata-bound Cu–(Ag) deposits: an overview. In: Porter, T.M. (Ed.), Hydrothermal Iron Oxide Copper–Gold & Related Deposits. A Global Perspective. PGC Publishing, Adelaide, 185-205.
Maksaev, Victor, Townley, Brian, Palacios, Carlos, Camus, Francisco, 2007. In: The Geology of Chile. The Geological Society of London, pp. 179–199. https://doi.org/10.1144/GOCH.6.
Manning, D.A.C. and Gize, A.P., 1993. The Role of Organic Matter in Ore Transport Processes; in Engel, M.H, and Macko, S.A. (Eds.), Organic Geochemistry, Principles and Applications, Chapter 5, 547-563.
Marikos, M.A., Laudon, R.C., Leventhal, J.S., 1986. Solid insoluble pyrobitumen in the Magmont West Orebody, Southeast Missouri. Econ. Geol. 81, 1983–1988.
Maureira, I., 2018. Estudio comparativo entre los depósitos Altamira y Las Luces, Cordillera de la Costa, Región de Antofagasta: Implicancias para el origen de los depósitos estratoligados de Cu – (Ag). Tesis de Magister, Universidad de Chile. (In Spanish, http://repositorio.uchile.cl/handle/2250/151836).
Masegosa R.M., Cañamero, P., Sánchez Cabezudo, M., Viñas, T., Salom, C., Prolongo, M. G., Páez, A., Ayala, M., 2012. Thermal behavior of bitumen modified by sulphur addition. 5th Eurasphalt & Eurobitumen Congress, Istanbul.
Mastalerz, M., Glikson, M., 2000. In-situ analysis of solid bitumen in coal: examples from the Bowen Basin and the Illinois Basin. Int. J. Coal Geol. 42, 207–220.
Mathur, R., Falck, H., Belogub, E., Milton, J., Wilson, M., Rose, A., Powell W., 2018. Origins of Chalcocite Defined by Copper Isotope Values. Geofluids, p. 9.
Mayer, C.K., Fontboté, L., 1990. The stratiform Ag-Cu deposit El Jardín, Northern Chile. In: Fontboté, L., Amstutz, G.C., Cardozo, M., Cedillo, E., Frutos, J. (Eds.), Stratabound Ore Deposits in the Andes. Springer, Berlin, pp. 637–646.
Migdisov, A.A., Guo, X., Williams-Jones, A.E., Sun, C.J., Vasyukova, O., Sugiyama, I., Fuchs, S., Pearce, K., Roback, R., 2017. Hydrocarbons as ore fluids. Geochem. Perspect. Let. 5, 47–52.
Mossman, D., Nagy, B., Davis, D., 1993. Hydrothermal alteration of organic matter in uranium ores, Elliot Lake, Canada: implications for selected organic-rich deposits. Geochim. Cosmochim. Acta 57, 3251–3259.
Munz, I.A., 2001. Petroleum inclusions in sedimentary basins: systematics, analytical methods and applications. Lithos 55, 195–212.
Naranjo, J., 1978. Geología de la zona interior de la Cordillera de la Costa entre los 26°20' Sur, Región de Atacama. Carta Geológica de Chile, escala 1:100.000. Instituto de Investigaciones Geológicas 34, 48 (in Spanish).
Naranjo, J., Puig, A., 1984. Hojas Taltal y Chañaral, Regiones de Antofagasta y Atacama, escala 1: 250.000, Carta Geológica de Chile N° 62-63 (in Spanish).
Oliveros, V., Féraud, G., Aguirre, L., Fornari, M., Morata, D., 2006. The early Andean magmatic province (EAMP): $^{40}Ar/^{39}Ar$ dating on Mesozoic volcanic and plutonic rocks from the Coastal Cordillera, Northern Chile. J. Volcanol. Geotherm. Res. 157 (4), 311–330.
Oliveros, V., Féraud, G., Aguirre, L., Ramírez, L., Fornari, M., Palacios, C., Parada, M., 2008. Detailed $^{40}Ar/^{39}Ar$ dating of geologic events associated with the Mantos Blancos copper deposit, northern Chile. Miner. Depos. 43 (3), 281–293.
Pfaff, K., Hildebrandt, L.H., Leach, D.L., Jacob, D.E., Markl, G., 2010. Formation of the Wiesloch Mississippi Valley-type Zn-Pb-Ag deposit in the extensional setting of the Upper Rhinegraben, SW Germany. Miner. Depos. 45 (7), 647–666.
Parnell, J., 1988. Metal enrichments in solid bitumens: a review. Miner. Depos. 23, 191–199.
Parnell, J. 1993. Bitumens in ore deposits. Special Publication No. 9 of the Society for Geology Applied to Mineral Deposits, Springer-Verlag, p. 1-6.
Peabody, C.E., 1993. The association of cinnabar and pyrobitumen in mercury deposits of the california coast range. In: Parnell, J., Kucha, H., Landais, P. (Eds.), Pyrobitumens in Ore Deposits, Special Publication No.9 of the Society of Geology Applied to Mineral Deposits. Springer-Verlag, Berlin, pp. 178–209.
Philippi, G.T., 1965. On the depth, time and mechanism of petroleum generation. Geochim. Cosmochim. Acta 29, 1021–1049.
Pérez, C.A., Radtke, M., Sanchez, H.J., Tolentino, H., Neuenshwander, R.T., Barg, W., Rubio, M., Bueno, M.I.S., Raimundo, I., Rohwedder, J.J.R., 1999. Synchrotron radiation X-ray fluorescence at the LNLS: beamline instrumentation and experiments. X-ray Spectrom. 28, 320–326.
Pichowiak, S., Buchelt, M., Damm, K.W., 1990. Magmatic activity and tectonic setting of the early stages of the Andean cycle in northern Chile. Geol. Soc. Am. Sp. Pub 241, 127–144.
Pomerantz, A.E., Bake, K.D., Craddock, P.R., Kurzenhauser, K.W., Kodalen, B.G., Mitra-Kirtley, S., Bolin, T.B., 2014. Sulfur speciation in kerogen and bitumen from gas and oil shales. Org. Geochem. 68, 5–12.
Pratt, L.M., Warner, M., 1998. Roles of organic matter in shales and carbonate hosted base metal deposits; in Kettler, R.M., Giordano, T.H., and Wood, S.Z. (Eds.), Ore genesis and Exploration: The roles of Organic Matter, SEG Short Course.
Reich, M., Chryssoulis, S.L., Deditius, A., Palacios, C., Zuñiga, A., Weldt, M., Alvear, M., 2010. "Invisible" silver and gold in supergene digenite. Geochim. Cosmochim. Acta 74, 6157–6173.
Reich, M., Palacios, C., Barra, F., Chryssoulis, S.L., 2013. "Invisible" silver in chalcopyrite and bornite from the Mantos Blancos Cu deposit, northern Chile. Eur. J. Mineral. 25, 453–460.
Riazi, M.R., Nasimi, N., Roomi, Y.A., 1999. Estimation of sulfur content of petroleum products and crude oils. Ind. Eng. Chem. Res. 38 (11), 4507–4512.
Richoz, S., van de Schootbrugge, B., Pross, J., Püttmann, W., Heunisch, C., Fiebig, J., Schouten, S., Wignall, P.B., 2012. Hydrogen sulphide poisoning of shallow seas following the end-Triassic extinction. Nat. Geosci. 5, 662–667.
Rieger, A., Schwark, L., Cisternas, M.E., Miller, H., 2008. Genesis and evolution of bitumen hosted in Lower Cretaceous lavas and its implications for strata-bound copper deposits, north Chile. Econ. Geol. 103, 387–404.
Robb, L.J., Meyer, F.M., 1995. The Witwatersrand Basin, South Africa: geological framework and mineralization processes. Ore Geol. Rev. 10, 67–94.
Rospondek, M., Leeuw, J., Baas, M., Bergen, P., Leereveld, H., 1994. The role of organically bound sulphur in stratiform ore sulphide deposits. Org. Geochem. 21 (12), 1181–1191.
Saintilan, N.J., Spangenberg, J.E., Chiaradia, M., Chelle-Michou, C., Stephens, M.B., Fontboté, L., 2019. Petroleum as source and carrier of metals in epigenetic sediment-hosted mineralization. Sci. Rep. 9, 8283.
Saric, N., Kreft, C., Huete, C., 2003. Geología del yacimiento Lo Aguirre. Rev. Geol. Chile 30, 2 (in Spanish).
Scheuber, E., Gonzalez, G., 1999. Tectonics of the Jurassic-Early Cretaceous magmatic arc of the north Chilean Coastal Cordillera (22°–26°S): a story of crustal deformation along a convergent plate boundary. Tectonics 18, 895–910.
Sjöblom, J., 2001. Encyclopedic Handbook of Emulsion Technology. Marcel Dekker, New York.
Speight, J.G., 1991. The chemistry and technology of petroleum, 2nd ed. Marcel Dekker Inc, New York.
Spirakis, C.S., 1996. The roles of organic matter in the formation of uranium deposits in sedimentary rocks. Ore Geol. Rev. 11, 53–69.
Sun, Y.Z., Püttmann, W., 2000. The role of organic matter during copper enrichment in Kupferschiefer from the Sangerhausen basin, Germany. Org. Geochem. 31 (11), 1143–1161.
Tissot, B.P., Welte, D.H., 1984. Petroleum Formation and Occurrence, 2nd ed. Springer-Verlag, Berlin Heidelbergd GmbH, New York.
Ulriksen, C., 1979. Regional geology, geochronology, and metallogy of the Coastal Cordillera between 23°30' and 26°S [Thesis]: Halifax, Nova Scotia, Dalhousie University, 180.
Watkinson, P., 2007. Deposition from crude oils in heat exchangers. Heat Transfer Eng. 28, 177–184.
Wedepohl, K.H., 1978. Handbook of Geochemistry 11, Sections 73. Springer-Verlag, B-G.
Wilson, N.S.F., 1998. The role of petroleum in the formation of the Soldado copper deposit, Chile: Hydrothermal replacement of a biodegraded petroleum reservoir. Unpublished Ph.D. thesis, Halifax, Canada, Dalhousie University, p. 418.
Wilson, N., Zentilli, M., 1999. The role of organic matter in the genesis of the El Soldado Volcanic-Hosted Manto-Type Cu Deposit, Chile. Econ. Geol. 94, 1115–1136.
Wilson, N., Zentilli, M., 2006. Association of pyrobitumen with copper mineralization from the Uchumi and Talcuna districts, central Chile. Int. J. Coal Geol. 65 (1), 158–169.
Wilson, N., Zentilli, M., Reynolds, P.H., Boric, R., 2003a. A age of mineralization by basinal fluids at the El Soldado manto-type copper deposit, Chile $^{40}Ar/^{39}Ar$ geochronology of K-feldespar. Chem. Geol. 197, 161–176.
Wilson, N., Zentilli, M., Spiro, B., 2003b. A sulfur, carbon, oxygen, and strontium isotope

study of the volcanic-hosted El Soldado manto type copper deposit, Chile: the essential role of bacteria and petroleum. Econ. Geol. 98, 163–174.
Wu, Y., Evans, K., Fisher, L.A., Zhou, M., Hu, S., Fougerouse, D., Large, R., Li, J., 2020. Distribution of trace elements between carbonaceous matter and sulfides in a sediment-hosted orogenic gold system. Geochim. Cosmochim. Acta 276, 345–362.
Zamora, A., 2011. Geología Proyecto Las Luces. Internal report. Compañía Minera Las Cenizas.
Zentilli, M., Boric, R., Munizaga, F. and Graves, M.C., 1994. Petroleum involvement in the genesis of some strata-bound copper deposits of Chile. Proceedings, 7th Chilean Geological Congress, Concepcion, Chile, II, 1542-1546.
Zentilli, M., Munizaga, F., Graves, M.C., Boric, R., Wilson, N.S.F., Mukhopadhayay, P.K., Snowdon, L.T., 1997. Hydrocarbon involvement in the genesis of ore deposits: an example in Cretaceous strata-bound (manto-type) copper deposits of central Chile. Int. Geol. Rev. 39, 1–21.